UC Irvine
UC Irvine Previously Published Works

Title
Three-dimensional imaging flow cytometry: current trends and future perspectives.

Permalink
https://escholarship.org/uc/item/8sr031d3

Journal
Lab on a Chip

ISSN
1473-0197

Authors
Hua, Xuanwen
Mandracchia, Biagio
Ling, Zhi
et al.

Publication Date
2026-10-16

DOI
10.1039/d6lc00580b

Copyright Information
This work is made available under the terms of a Creative Commons Attribution License, available at https://creativecommons.org/licenses/by/4.0/

Peer reviewed

eScholarship.org Powered by the California Digital Library
University of California

Lab on a Chip

CRITICAL REVIEW

Published on 16 October 2026
Licensed under CC-BY-NC 4.0

Cite this: DOI: 10.1039/d6lc00580b

Three-dimensional imaging flow cytometry: current trends and future perspectives

Xuanwen Hua, †[abc] Biagio Mandracchia, †[d] Zhi Ling,†[abef] Kidan Tadesse,[abe] Hajun Yoo,[ab] Jin Yan,[g] Ho Wai Howard Lee[ghi] and Shu Jia *[abej]

Received 3rd July 2026,
Accepted 2nd October 2026

DOI: 10.1039/d6lc00580b

rsc.li/loc

Imaging flow cytometry (IFC) combines microscopic techniques and flow cytometry, enabling high-throughput, population-scale single-cell analysis with rich spatial detail and high molecular specificity. To date, most established IFC platforms are fundamentally built around 2D imaging, which is inherently limited in its ability to capture the complex 3D morphology, intracellular organization, and spatially distributed molecular features of single cells under flow. Driven by the growing demand for volumetric cellular information, IFC has progressively evolved from 2D imaging toward 3D imaging flow cytometry through a variety of optical and computational strategies. Existing 3D IFC approaches typically fall into scanning-based and non-scanning modalities, depending on whether volumetric information is assembled through sequential or parallel acquisition, with each paradigm offering complementary strengths in 3D imaging performance and cytometric throughput. Here, we systematically compare the underlying principles and performance characteristics of the most representative scanning-based and non-scanning 3D IFC technologies and discuss current challenges and future opportunities to advance volumetric cytometric analysis in biomedical and translational research.

1 Introduction

Three-dimensional imaging flow cytometry (3D IFC) aims to overcome a fundamental limitation of conventional imaging flow cytometry (IFC): the loss of axial information when inherently three-dimensional cellular structures are projected into two-dimensional images.[1,2] While IFC successfully combines the throughput of flow cytometry with the spatial resolution of microscopy,[3–7] it fundamentally compresses cellular organization into planar representations, obscuring subcellular architecture and spatial relationships. Recovering this missing dimensionality expands the space of measurable phenotypes, enabling direct access to intracellular organization, morphology, and dynamic processes at the single-cell level.[8]

On one hand, many cytometric measurements based primarily on integrated fluorescence intensity, marker abundance, cell counting, or coarse morphological features can be adequately addressed using conventional 2D IFC. On the other hand, volumetric imaging becomes particularly important when the phenotype of interest depends on the true three-dimensional geometry or axial arrangement of cellular structures and therefore cannot be uniquely inferred from a planar image. Representative examples include quantitative analysis of cell and nuclear morphology and deformation,[9–11] the organization and remodeling of intracellular organelles,[12–15] and the spatial localization of chromatin or internalized nanoparticles within the cellular volume.[16] In these cases, 2D projection can superimpose structures located at different depths, obscure axial relationships, and make morphometric measurements dependent on cell orientation, whereas access to the full volume enables direct quantification of three-dimensional shape, internal topology, and spatial heterogeneity.

These capabilities are particularly relevant when structural reorganization itself constitutes the biological readout. Volumetric IFC has therefore been applied to the

[a] Laboratory for Systems Biophotonics, Georgia Institute of Technology, Atlanta, GA, USA. E-mail: shu.jia@gatech.edu
[b] Wallace H. Coulter Department of Biomedical Engineering, Georgia Institute of Technology and Emory University, Atlanta, GA, USA
[c] Department of Medical Science and Innovation, SiRIUS Institute of Medical Research, Tohoku University, Sendai, Miyagi, Japan
[d] E.T.S.I. Telecomunicación, Universidad de Valladolid, Valladolid, Spain
[e] Parker H. Petit Institute for Bioengineering and Biosciences, Georgia Institute of Technology, Atlanta, GA, USA
[f] George W. Woodruff School of Mechanical Engineering, Georgia Institute of Technology, Atlanta, GA, USA
[g] Department of Physics & Astronomy, University of California, Irvine, California, USA
[h] Beckman Laser Institute and Medical Clinic, University of California, Irvine, California, USA
[i] Eddleman Quantum Institute, University of California, Irvine, California, USA
[j] Winship Cancer Institute, Emory University, Atlanta, GA, USA
† These authors contributed equally.

characterization of cell-state transitions and apoptosis, drug-induced remodeling and therapeutic response, intracellular delivery, and disease-associated phenotypes.[17–19] Label-free tomographic approaches further extend this concept by using three-dimensional refractive-index distributions to characterize intrinsic cellular and subcellular properties, including nuclear structure and other biophysical phenotypes, without exogenous labels.[20–22] Thus, the transition from 2D to 3D is most consequential when axial information changes the biological interpretation of morphology, localization, or intracellular organization, rather than merely providing a more complete visualization. The central motivation for 3D IFC is to make such volumetric phenotypes accessible at the population scale, combining the structural information of 3D microscopy with the statistical power and throughput of flow cytometry.

Realizing this biological objective requires bridging the gap between high-throughput cytometry and high-content imaging[23] through the integration of advanced optical imaging modalities with microfluidic systems. Achieving volumetric imaging in flow, however, introduces a central technological challenge: balancing spatial resolution, acquisition speed, and system complexity.[24] To address this trade-off, a range of complementary strategies has been developed. Optical sectioning approaches recover axial information by acquiring sequential focal-plane cross-sections, typically using custom microfluidic devices or tilted detection schemes.[25–28] These methods provide high axial resolution and strong sectioning contrast but rely on sequential acquisition, introducing constraints on throughput and synchronization with cell motion. In parallel, computational imaging strategies, including light-field-based and beam-engineered approaches, encode depth information into a single or reduced number of measurements, enabling volumetric reconstruction without explicit scanning.[29,30] In addition to fluorescence-based implementations, label-free

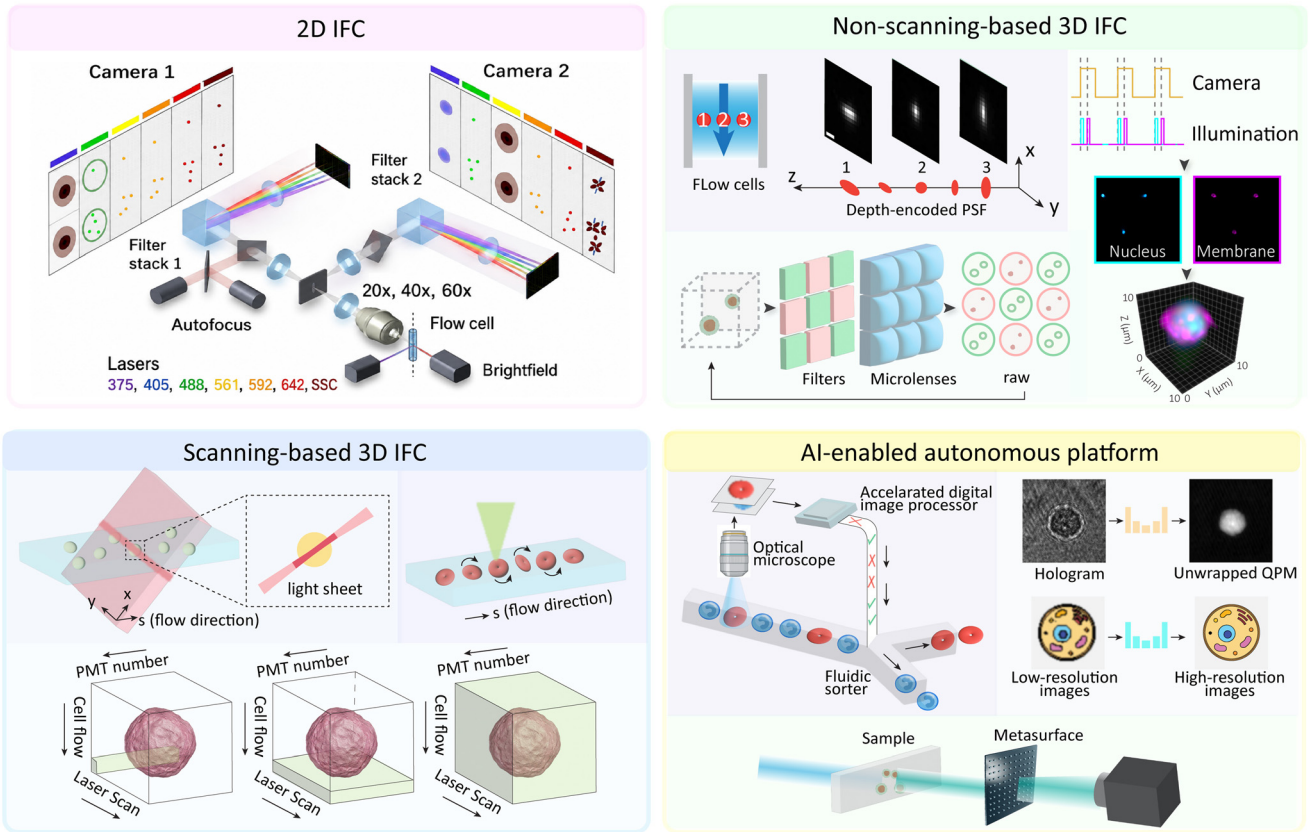


Fig. 1 Evolution of imaging flow cytometry (IFC) from 2D to advanced 3D platforms. Conventional 2D IFC combines high-throughput single-cell imaging with quantitative analysis (redrawn and adapted with background inverted from the ImageStreamX Mark II system specifications (Cytek Biosciences/Amnis), with reference to the underlying optical system reported in ref. 35). Scanning-based 3D IFC reconstructs cellular volumes through axial scanning or multi-view imaging of rotating cells (reproduced from ref. 36–38 with permission from J. Son *et al.*, *Lab Chip*, Royal Society of Chemistry, copyright 2023; F. Merola *et al.*, *Light: Sci. Appl.*, Springer Nature, copyright 2017; and M. Zhou *et al.*, *APL Photonics*, AIP Publishing, copyright 2025), whereas non-scanning 3D IFC enables instantaneous volumetric acquisition using depth-encoded point-spread functions (PSFs) or light-field angular encoding (reproduced from ref. 16–18 with permission from L. E. Weiss *et al.*, *Nat. Nanotechnol.*, Springer Nature, copyright 2020; X. Hua *et al.*, *Nat. Commun.*, Springer Nature, copyright 2024; and Z. Ling *et al.*, *Lab Chip*, Royal Society of Chemistry, copyright 2026). Emerging AI-enabled platforms further integrate automated image reconstruction, restoration, cell sorting, and compact metasurface-based imaging (adapted from ref. 39 and 40 with permission from T. Ding *et al.*, *Nat. Rev. Bioeng.*, Springer Nature, copyright 2025; and D. Pirone *et al.*, *Lab Chip*, Royal Society of Chemistry, copyright 2022).

This journal is © The Royal Society of Chemistry 2026

tomographic approaches reconstruct the three-dimensional refractive index distribution of cells, providing access to intrinsic biophysical properties such as mass density and internal organization.[31–34] While these methods extend cytometry beyond fluorescence contrast, they introduce additional challenges related to acquisition geometry, angular sampling, and reconstruction robustness under dynamic flow conditions.

Taken together, these approaches define a multidimensional trade space between spatial resolution, acquisition speed, and experimental complexity. Rather than converging toward a single architecture, we observe that 3D IFC technologies have evolved along two primary operational paradigms: scanning-based approaches, in which volumetric information is assembled through sequential acquisition, and non-scanning approaches, relying on parallel or computational encoding of depth information. Each paradigm offers distinct advantages and limitations in terms of imaging performance and cytometric throughput. Additionally, these 3D IFC modalities are increasingly integrated with AI-driven processing and autonomous control to bridge the gap between high-dimensional data acquisition and high-throughput data processing and decision-making (Fig. 1).

In the following sections, we first review scanning-based 3D IFC techniques, focusing on optical-sectioning strategies and their evolution toward higher throughput and improved integration. We then discuss non-scanning approaches that rely on multiplexed image acquisition, including multifocal, beam-engineered, and light-field-based methods, highlighting their potential for single-shot volumetric imaging in flow. Finally, we summarize the biological applications of these technologies, compare their key trade-offs, and discuss emerging opportunities for more compact, computationally integrated, and autonomous 3D IFC platforms.

2 Scanning-based 3D IFC techniques

Scanning-based 3D IFC techniques assemble volumetric information through sequential acquisition, encompassing optical sectioning, quantitative phase, and light-scattering modalities for acquisition of 3D morphology and subcellular organization in single cells under flow (Table 1).

2.1 Fluorescence-based optical-sectioning 3D IFC

Fluorescence-based optical-sectioning 3D IFC combines the molecular specificity of fluorescence microscopy with the ability to recover axial information from cells in flow. In these methods, three-dimensional information is obtained by sequentially acquiring a series of two-dimensional images from different focal or illumination planes as each cell moves through the imaging region. The main challenge is therefore not only to generate sufficient optical-sectioning contrast to reject out-of-focus fluorescence, but also to acquire enough axial samples before the cell leaves the field of view (FOV). Depending on the imaging modality and illumination geometry employed for optical sectioning, these techniques can be grouped into four main categories: regular wide-field, light-sheet and selective plane illumination, structured illumination, and confocal approaches (Fig. 2).

One of the simplest strategies exploits the translational motion of the flowing cell as a passive axial scanner. In tilted-channel configurations, the microfluidic channel is inclined with respect to the microscope focal plane, so that a cell progressively traverses different focal depths during its transit through the imaging region. Pégard and Fleischer first demonstrated this principle using wide-field 3D deconvolution microscopy in an obliquely oriented microfluidic channel.[41] Jagannadh *et al.* later refined this concept for fluorescence-based 3D IFC by fabricating precisely slanted microfluidic channels in glass using femtosecond laser inscription. Their implementation acquired approximately 200 optical sections per cell, corresponding to an effective axial sampling of ~15 nm, using a standard wide-field fluorescence microscope[28] (Fig. 2a). This strategy is attractive because it requires no moving optical elements, but its performance depends strongly on flow stability, cell trajectory, and accurate registration of the sequential image stack.

A complementary optical-sectioning strategy is light-sheet microscopy (LSM), which confines fluorescence excitation to a thin plane and thereby provides intrinsic optical sectioning, reduced background, improved photon efficiency, and lower phototoxicity compared with conventional wide-field illumination. Early light-sheet-based IFC demonstrations by Wu *et al.* showed volumetric reconstruction of phytoplankton chlorophyll-a structures from sequential light-sheet cross-sections[42] (Fig. 2b). This study established LSM as a natural platform for 3D IFC because the motion of the cell through the light sheet can be used to build a volumetric image stack with high optical-sectioning contrast.

Subsequent advances in LSM-based 3D IFC have focused on improving sectioning efficiency, throughput, and compatibility with microfluidic operation. On the illumination side, lattice light-sheet excitation has been introduced to reduce background fluorescence and phototoxicity while improving axial confinement[43] (Fig. 2c). Other approaches have increased imaging speed by engineering the excitation pattern or parallelizing the illumination, enabling simultaneous interrogation of multiple axial layers or multiple flowing cells without relying on slow beam dithering[15,47,48] (Fig. 2d). In parallel, detection schemes have been adapted to the speed–sensitivity–sectioning trade-off that is intrinsic to flow-based imaging. Examples include extended-depth-of-focus detection using an acoustic tunable lens[47] and acoustofluidic focusing to confine cells to a narrow and reproducible stream within the camera FOV[27] (Fig. 2e).

More recent studies have progressively transitioned LSM-based 3D IFC from externally aligned bulk-optical

Table 1 Comparison of representative scanning-based 3D imaging flow cytometry implementations

Methods	Acquisition	Resolution	Throughput	Labeling	Reconstruction	Computational burden	System complexity	Applications
Tilted/slanted-channel wide-field[28,41]	Passive scan in inclined status	*XY*: diff. limited, *Z*: ~1–2 μm; *XY*: 0.37 μm, *Z*: 1.9 μm	0.3 cells per s; 200 fps (camera limited)	Brightfield; fluorescence	3D deconvolution	Moderate	Low – static wide-field optics	3D cell morphology
Light-sheet[42]	Flow through static light sheet	*XY*: 0.8 μm, *Z*: 1.4 μm	35–44 cells per s	Fluorescence	Direct stack assembly	Low	Moderate – light-sheet illumination	3D chlorophyll-a architecture; phytoplankton taxonomy
Lattice light-sheet[43]	Lattice-sheet excitation with flow-driven sectioning	*XY*: 300–350 nm, *Z*: 1.2–1.6 μm	N.A., camera-limited	Fluorescence	Stack assembly + deconvolution	Moderate	High – lattice light-sheet generation	Low-phototoxicity subcellular imaging
Spatio-temporal-transform/parallel oblique-plane LSM[26,27]	All planes in one exposure; multi-channel	*XY*: 0.88 μm, *Z*: 1.34 μm; *XY*: ~0.6 μm, *Z*: ~1.0–2.5 μm	>2000 cells per s	Fluorescence	Remapping, deskewing & stacking	Moderate	Moderate to high – tilted single-objective sheet	Volumetric phenotyping, mitotic-phase discrimination
iLIFE[12,14]/VFC[13]/M3IC light-sheet volume cytometry[15]	Passive scanning; orthogonal detection, multi-channel parallelization	*XY*: 2–5 μm, *Z*: 3–5 μm	~5–23 cells per s	Fluorescence	Deconvolution with shift-correction & stacking	Moderate	Moderate to high – multi-channel configuration	Quantitative organelle phenotyping; drug response; whole-organism imaging
Confocal[44,45]	Point-array scanning with single-pixel detection	*XY*: 0.4–0.7 μm; *Z*: 5.8 μm	10 000–20 000 cells per s	Fluorescence	Digital demodulation	Low to moderate	High – acousto-optic beam generation, QAM electronics, scanning optics	3D micro-organism motility; cell classification
Holo-tomography/ODT in flow[19,20,34,37,40]	Angular diversity from cell rotation, line-beam translation	Rotation-limited	~1.67 cells per s; up to tens per s	Label-free	Orientation recovery & tomographic inversion; CNN-accelerated	High	Moderate – off-the-shelf interferometer & straight channel	Cell/organelle phenotyping & characterization
Side-scattering single-pixel imaging[25,46]	Light sheet sweeps in *z*, flow scans in *y* & spatial filter encoding	*X*: 1 μm, *Y*: 2 μm, *Z*: 2 μm	~500 cells per s	Fluorescence & brightfield	Time-voxel remapping; 3D CNN	Moderate	Moderate – AOD, custom spatial filter, multi-PMT	Label-free phenotyping; volumetric scattering-fingerprint classification
Forward-scattering[38]	AOD scanning, flow scanning, & spatial filter transformation	*XY*: 1.5 μm, *Z*: 2.5 μm	400 cells per s	Label-free	Spatio-temporal deconvolution	Moderate	Moderate to high – beam shaping, AOD, micro-mirror array & 8-channel PMT	Label-free morphology, size & RI-gradient screening

This journal is © The Royal Society of Chemistry 2026

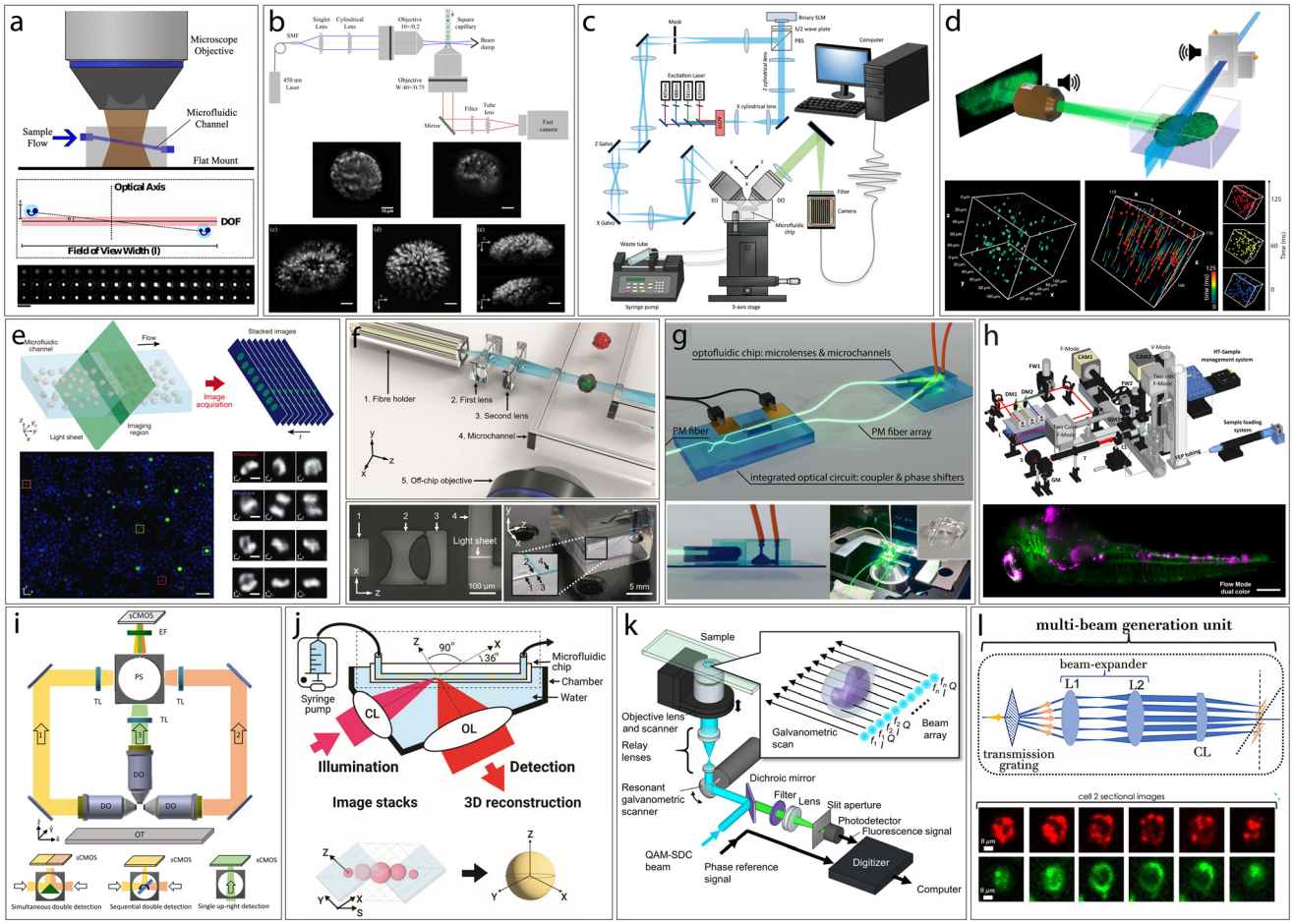


Fig. 2 Fluorescence optical-sectioning-based 3D IFC techniques. (a) A slanted channel microfluidic chip for 3D fluorescence imaging of cells in flow (reproduced from ref. 28 with permission from V. K. Jagannadh *et al.*, *Opt. Express*, Optica Publishing Group, copyright 2016). (b) A light-sheet fluorescence imaging flow cytometer for 3D sectioning of phytoplankton (reproduced from ref. 42 with permission from J. Wu *et al.*, *Opt. Express*, Optica Publishing Group, copyright 2013). (c) A lattice light-sheet microscopy-based microfluidic platform sealed with a thin, water-refractive-index-matched film to reduce light scattering (reproduced from ref. 43 with permission from Y. J. Fan *et al.*, *Lab Chip*, Royal Society of Chemistry, copyright 2021). (d) Inertia-free light-sheet flow cytometry using an acousto-optic scanner for tailored illumination and an acoustic-optofluidic lens for extended depth (reproduced from ref. 47 with permission from M. Duocastella *et al.*, *ACS Photonics*, American Chemical Society, copyright 2017). (e) Fast, parallel optofluidic scanning with 1D acoustofluidic focusing of multiple cells under wide-field light-sheet microscopy enables high throughput (reproduced from ref. 27 with permission from M. Ugawa and S. Ota, *Small Sci.*, Wiley-VCH, copyright 2022). (f) An optofluidic light-sheet system flows suspended cells through a light sheet formed by micro-optical components cast directly in polydimethylsiloxane (PDMS) (reproduced from ref. 49 with permission from E. J. Vargas-Ordaz *et al.*, *Lab Chip*, Royal Society of Chemistry, copyright 2021). (g) An integrated optofluidic platform generates structured light-sheet illumination within a microchannel, enabling enhanced-resolution 3D imaging of flowing cells (reproduced from ref. 7 with permission from P. Paie *et al.*, *Lab Chip*, Royal Society of Chemistry, copyright 2024). (h) An open-source Arduino-MicroManager platform enables automated, high-throughput 3D light-sheet imaging of cell cultures and model organisms for large-scale drug screening (reproduced from ref. 52 with permission from E. J. Gualda *et al.*, *Biomed. Opt. Express*, Optica Publishing Group, copyright 2015). (i) Modular light-sheet microscope with switchable modalities for classical and high-throughput imaging (reproduced from ref. 53 with permission from M. Bernardello *et al.*, *Sci. Rep.*, Springer Nature, copyright 2022). (j) Portable light-sheet optofluidic microscopy employs a compact, open-top configuration compatible with commonly adopted microfluidic chips (reproduced from ref. 36 with permission from J. Son *et al.*, *Lab Chip*, Royal Society of Chemistry, copyright 2023). (k) Confocal microscopy with spatial dual-comb and quadrature amplitude modulation enables frequency-division multiplexed excitation and single-pixel detection for ultrafast imaging (reproduced from ref. 45 with permission from H. Mikami *et al.*, *Chem*, Elsevier, copyright 2018). (l) Multifunctional (multichannel, multisheet and multicolor) imaging cytometry (M3IC) system that employs vertically-aligned multi-sheet array illumination for interrogating cells flowing simultaneously through multiple microfluidic channels (reproduced from ref. 15 with permission from P. Joshi *et al.*, *Commun. Phys.*, Springer Nature, copyright 2024).

implementations toward compact optofluidic platforms in which light-sheet generation, beam delivery, and microfluidic sample handling are co-integrated on chip. Early demonstrations established the feasibility of embedding micro-optical elements directly within PDMS-based microfluidic devices to achieve self-aligned and mechanically stable light-sheet excitation[49] (Fig. 2f). Glass-based microscope-on-chip platforms further improved

robustness by integrating microchannels, optical coupling structures, and light-sheet-forming microlenses within a single substrate.[50] More recent implementations have moved beyond passive miniaturization by incorporating active optical control, phase modulation, structured light-sheet generation, photonic circuits, waveguides, and flow channels within unified optofluidic architectures[7,51] (Fig. 2g). These developments illustrate how optical integration can reduce alignment complexity while enabling more reproducible and scalable 3D IFC systems.

In parallel, the development of LSM-based 3D IFC has also improved platform compatibility and experimental feasibility through the implementation of open-source, modular, and portable architectures. Earlier innovations, such as the SPIM-fluid platform, utilized open-source hardware and software control to automate high-throughput 3D imaging for a range of samples-from 3D cell cultures to whole organisms-thereby enhancing system accessibility for large-scale screenings[52] (Fig. 2h). To address the limitations of application-specific setups, subsequent modular designs have significantly increased system compatibility by combining classical, flow-based, and hybrid acquisition modes within a single instrument, enabling users to switch between long-term imaging, multicolor imaging, and higher-throughput screening while maintaining the freedom of implementing additional detection add-ons and diverse specimen types[53] (Fig. 2i). More recently, the introduction of portable systems with open-top light-sheet configurations has further improved flexibility for easy deployment with minimized instrumental complexity[36] (Fig. 2j). These advancements in compact design and cost-effective hardware have lowered the barriers for broad dissemination and facilitated the integration of 3D IFC into diverse high-content biological research pipelines.

Confocal microscopy provides an alternative route to fluorescence optical sectioning by combining point-scanning illumination with pinhole-filtered detection, effectively rejecting out-of-focus light to yield high axial resolution. In flow-based implementations, the motion of the cell can again provide one component of the volumetric scan, analogous to tilted-channel wide-field imaging. Quint *et al.* demonstrated this strategy in 2017, integrating a confocal laser-scanning microscopy to obtain 3D tomograms of red blood cells under physiologically relevant flow conditions.[9] However, conventional confocal 3D IFC is limited by point-scanning speed, fluorescence lifetime, and the need to maintain adequate signal-to-noise ratio at high flow velocities. Mikami *et al.* addressed these limitations by introducing an ultrafast confocal fluorescence microscopy approach based on frequency-division multiplexing, using a frequency-comb-referenced swept laser and optical fiber delays to achieve scan rates beyond the conventional fluorescence-lifetime limit[45] (Fig. 2k).

Over the past decades, these system-level advances have led to a substantial three-order-of-magnitude increase in volumetric throughput while simultaneously narrowing the resolution gaps among various microscopic modalities. Early light-sheet systems established baselines of 35–44 cells per s with ~0.8 μm lateral and ~1.4 μm axial resolution.[42] However, the throughput was fundamentally limited to a few hundred cells per minute by the intrinsic coupling between flow speed and camera readout, as sufficient cross-sectional sampling for each cell is required to enable accurate 3D reconstruction.[42] One key strategy encodes all cross-sections into a single camera exposure *via* spatiotemporal transformation, eliminating the frame-rate limit and enabling 3D reconstruction at flow velocities exceeding 10 m s^{-1}.[26] Building on this, a stationary oblique-plane geometry parallelized across multiple channels scaled 3D acquisition to over 2000 cells per s.[27] Parallel developments have focused on organelle-level volumetric readout in flowing cells, beginning with the integrated light-sheet flow cytometry (iLIFE) platform.[12] This approach was subsequently advanced to achieve real-time volumetric reconstruction of mitochondria in HeLa cells[13] and multicolor tracking for quantifying drug-induced remodeling.[14] Most recently, the introduction of multi-sheet illumination arrays has enabled simultaneous organelle-level readout across parallel microfluidic streams[15] (Fig. 2l). Meanwhile, in the confocal domain, frequency-division-multiplexed scanning has successfully bypassed the fluorescence-lifetime limit, enabling 3D confocal cytometry at flow speeds of up to 2 m s^{-1}.[44] Regarding spatial resolution, the adoption of lattice light-sheet profiles has significantly tightened axial confinement while reducing phototoxicity compared to standard Gaussian sheets.[43] Furthermore, the integration of structured illumination *via* glass-inscribed photonic circuits has extended lateral resolution beyond the diffraction limit in an alignment-free, chip-scale format.[7,51]

Despite these advances, fluorescence optical-sectioning 3D IFC remains constrained by several practical trade-offs. Increasing flow speed reduces residence time in the imaging region and therefore limits axial sampling unless acquisition is parallelized or encoded. Improving axial resolution often requires thinner light sheets, tighter confocal gating, or denser sampling, all of which can reduce photon budget or throughput. Multicolor and organelle-level imaging further increase the demands on illumination power, detector sensitivity, spectral separation, and computational reconstruction. Consequently, future progress will likely depend on co-optimizing microfluidic control, illumination geometry, detector architecture, and reconstruction algorithms rather than improving any single component in isolation.

2.2 Volumetric quantitative phase IFC

The ongoing evolution of IFC is increasingly driven by the need to move beyond fluorescence-based contrast toward label-free, quantitative, and high-content analysis.[54,55] Fluorescence contrast is particularly useful for imaging

 This journal is © The Royal Society of Chemistry 2026

labeled cells, organelles, or molecular targets, but it also imposes additional constraints compared with label-free imaging, including its reliance on labeling, photobleaching, and limited multiplexing constrains its applicability in dynamic, long-term, or clinically sensitive measurements.[56–58] In response, a new class of label-free imaging modalities has emerged, leveraging intrinsic optical properties of cells—primarily refractive index (RI) and optical phase—to enable quantitative characterization without exogenous markers.[31,59] Within this framework, label-free IFC represents a rapidly developing frontier, combining microfluidics, computational imaging, and

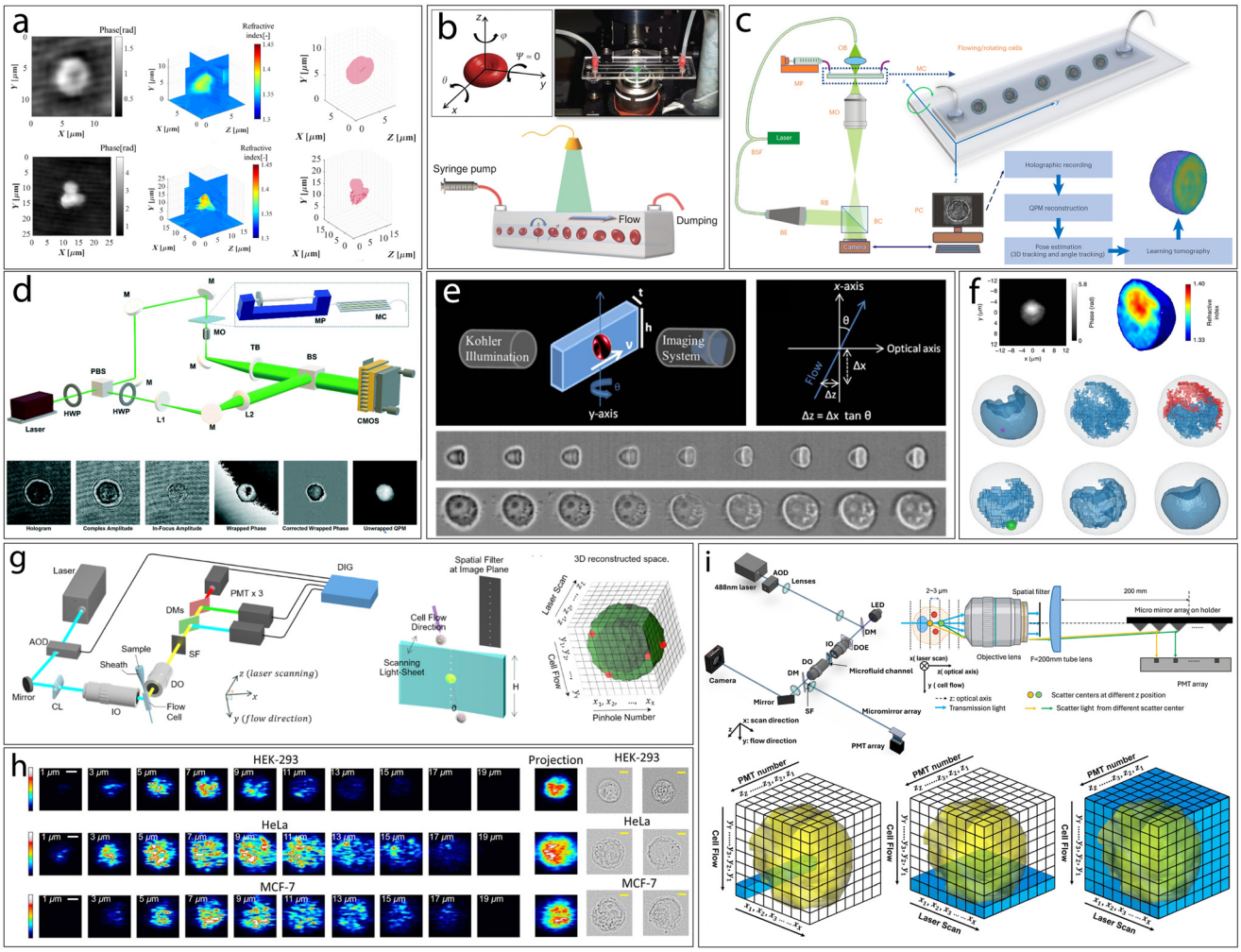


Fig. 3 Holographic and scattering-based 3D IFC. (a) Three-dimensional quantitative phase imaging flow cytometry of blood coagulation structures by optical projection tomography using digital holographic microscopy (reproduced from ref. 66 with permission from H. Funamizu and Y. Aizu, *J. Biomed. Opt.*, SPIE, copyright 2018). (b) Stain-free 3D refractive index (RI) tomograms of flowing and rotating single cells reconstructed from multiple digital holograms recorded around the cell using the inverse Radon transform (reproduced from ref. 37 with permission from F. Merola *et al.*, *Light: Sci. Appl.*, Springer Nature, copyright 2017). (c) Label-free identification of cell nuclei from reconstructed 3D RI tomograms using tomographic phase microscopy in flow cytometry (reproduced from ref. 20 with permission from D. Pirone *et al.*, *Nat. Photonics*, Springer Nature, copyright 2022). (d) Processing pipeline incorporating a multi-scale fully convolutional context aggregation network that accelerates reconstruction of phase-contrast tomograms in holographic flow cytometry (reproduced from ref. 40 with permission from D. Pirone *et al.*, *Lab Chip*, Royal Society of Chemistry, copyright 2022). (e) Transport-of-intensity (TIE)-based phase imaging flow cytometry collects focal stacks for 3D reconstruction (reproduced from ref. 77 with permission from S. S. Gorthi and E. Schonbrun, *Opt. Lett.*, Optica Publishing Group, copyright 2012). (f) Holo-tomographic flow cytometry enables phenotypic profiling of leukemia blast cells to identify mutation-associated cellular features (reproduced from ref. 19 with permission from D. Pirone *et al.*, *Light: Sci. Appl.*, Springer Nature, copyright 2025). (g) 3D side-scattering imaging flow cytometry combines orthogonal light-sheet scanning illumination with spatiotemporal transformation detection to reconstruct 3D cell images from a cameraless single-pixel photodetector readout (reproduced from ref. 25 with permission from Y. Han *et al.*, *Optica*, Optica Publishing Group, copyright 2019). (h) Convolutional neural network (CNN) analysis for classification on 3D side-scattering cell images out of a unique 3D imaging flow cytometer study (reproduced from ref. 46 with permission from R. Tang *et al.*, *APL Photonics*, AIP Publishing, copyright 2020). (i) 3D forward-scattering imaging flow cytometry system employs optical needle-beam illumination, linear micro-mirror arrays for axial scatter detection, and spatiotemporal deconvolution algorithms to achieve label-free single-cell 3D imaging (reproduced from ref. 38 with permission from M. Zhou *et al.*, *APL Photonics*, AIP Publishing, copyright 2025).

advanced optical methods to deliver volumetric information at high throughput.

The fundamental optical principle underlying most label-free IFC techniques is quantitative phase imaging (QPI), namely the capability to simultaneously measure the phase delay induced by a specimen as light propagates through it. Since the phase shift is directly related to the optical path length, QPI provides access to physically meaningful quantities such as dry mass, intracellular density, and RI distribution.[60] Compared to intensity-based imaging, phase contrast is particularly well suited for transparent biological samples, enabling high-sensitivity detection of subtle morphological and biophysical variations. This capability has driven a substantial convergence between QPI and flow cytometry, enabling the development of diverse dynamic, high-throughput implementations compatible with microfluidic platforms, and spanning a broad range of length scales, methodologies, and applications.[61,62]

Digital holography represents one of the most mature and widely adopted implementations of QPI in flow cytometry. By recording the interference between a reference and an object beam, it enables single-shot reconstruction of the complex optical field, from which both amplitude and phase can be numerically retrieved.[20] This capability is particularly advantageous under flow conditions, where high throughput and minimal acquisition times are essential.[63,64] Importantly, holography is inherently compatible with three-dimensional reconstruction when multiple perspectives of the specimen are available, providing a natural pathway toward volumetric characterization.[65] This extension toward volumetric imaging is generally realized through Optical Diffraction Tomography (ODT), also referred to as holotomography. ODT reconstructs the three-dimensional refractive index (RI) distribution of a specimen from multiple angular projections, in close analogy to X-ray computed tomography.[32] In conventional implementations, angular diversity is achieved through mechanical rotation of the sample or by varying the illumination angle, both of which are challenging to implement in flow cytometry settings. However, within microfluidic environments, cells frequently undergo spontaneous rotation due to shear gradients in laminar flow. This intrinsic rotational motion can be exploited to acquire multiple views of the same cell, enabling tomographic reconstruction of volumetric RI maps without the need for external mechanical manipulation[34,37,66] (Fig. 3a and b).

Despite its promise, volumetric QPI and ODT in flow still face some limitations. For example, tomographic reconstruction requires sufficient sampling of the object from different viewing angles. In practice, the finite numerical aperture of the imaging system and restricted angular coverage leave part of the three-dimensional spatial-frequency spectrum unmeasured, giving rise to the well-known missing-cone problem.[67] This results in anisotropic resolution, axial elongation of reconstructed structures, and potential underestimation or distortion of refractive-index (RI) values. These effects can be particularly important in flow-based implementations, where the number and distribution of available views are constrained by the short observation time and, when cell rotation is exploited, by the often non-uniform and only partially controlled rotational dynamics of individual cells. Errors in estimating the instantaneous orientation of a rapidly translating or rotating cell, together with motion blur and sparse angular sampling, can therefore propagate directly into the reconstructed 3D RI distribution.[68]

Another limitation arises from the physical model used for reconstruction. Most conventional ODT approaches rely on linearized wave-scattering models based on the Born or Rytov approximations,[69,70] and neglect high-order multiple scattering. These approaches are effective for weakly scattering specimens, but their accuracy deteriorates for optically thick or strongly scattering samples and for structures with large RI contrast.[71] Under these conditions, multiple scattering becomes significant, and the measured field can no longer be adequately described by the simplified forward model, resulting in distortions and quantitative errors in the reconstructed RI distribution. Nonlinear inverse-scattering and multiple-scattering models can improve reconstruction fidelity, but at the cost of substantially greater computational complexity.[72] This trade-off is especially relevant to IFC, where reconstruction must ultimately be compatible with high acquisition rates and large numbers of cells.

Recent work has addressed such limitations to further advance flow-based tomography by improving rotation control, angular coverage, and reconstruction fidelity. Strategies based on hydrodynamic focusing,[73] inertial microfluidics,[74] and tailored channel geometries[24] have been proposed to enhance cell orientation and rotational dynamics, thereby mitigating the missing-angle problem and improving axial resolution. In parallel, computational reconstruction methods are increasingly used to compensate for limited-angle sampling, noise, and model inaccuracies, enabling high-quality reconstructions from sparse measurements and opening the door to real-time volumetric imaging[20,40,75] (Fig. 3c and d). More advanced inverse-problem approaches can also explicitly account for multiple light scattering. For example, iterative solvers based on modified Born series[76] can extend quantitative reconstruction beyond the weak-scattering regime, achieving both accuracy and computational efficiency simultaneously.

Beyond holographic approaches, non-interferometric QPI methods such as transport-of-intensity equation (TIE) imaging have gained increasing attention due to their simpler optical configurations and robustness to noise.[78] TIE-based techniques reconstruct the phase from intensity variations along the optical axis, typically using defocused images acquired at different planes.[79] Compared to holography, TIE approaches offer reduced system complexity and improved stability, albeit often at the cost of requiring multiple measurements or reduced temporal resolution[77]

 This journal is © The Royal Society of Chemistry 2026

(Fig. 3e). Recent developments in dual-view and real-time TIE implementations have alleviated these limitations by enabling phase retrieval from minimal datasets that can be acquired simultaneously.[80,81] Although these approaches do not directly provide volumetric refractive-index reconstructions, their high-speed, label-free phase measurements make them particularly attractive for imaging flow cytometry and potentially complementary to tomographic strategies.

The convergence of these techniques highlights a broader trend toward computationally enhanced imaging in IFC. Rather than relying solely on optical hardware, these approaches distribute complexity between acquisition and reconstruction, enabling flexible trade-offs between speed, resolution, and system simplicity.

However, the nature of the contrast itself can impose additional limitations. Although 3D RI maps provide quantitative, label-free information, RI contrast lacks the molecular specificity provided by targeted labeling. Different cellular components may exhibit similar or overlapping RI values, making the unambiguous identification of specific proteins, organelles, or biochemical species substantially more difficult than with fluorescence-based approaches. ODT is therefore better regarded as complementary to, rather than a universal replacement for, fluorescence-based IFC. Despite this limitation, volumetric QPI in flow offers important opportunities in both biological and physico-chemical systems. It has been repeatedly demonstrated that 3D RI maps can provide sufficient intrinsic contrast for the label-free characterization of several subcellular structures, particularly nuclei and lipid droplets in a statistically robust manner[19–22,66,82–85] (Fig. 3f). In parallel, similar techniques have been applied to non-biological systems, where 3D phase imaging enables *in situ* measurement of concentration fields, mixing dynamics, and interfacial phenomena.[86,87]

Looking forward, the field is expected to benefit from the continued integration of optofluidics, computational imaging, and artificial intelligence. Advances in microfluidic design can enhance cell rotation, alignment, and focusing, improving the quality of tomographic reconstructions and cell throughput.[88] At the same time, deep learning approaches are increasingly being used to accelerate phase retrieval, correct reconstruction artifacts, and perform end-to-end classification directly from raw optical data.[89–94] In this emerging paradigm, label-free 3D IFC becomes not only an imaging modality but a data-rich sensing platform, where quantitative optical measurements are tightly coupled to computational inference.

From a broader perspective, label-free 3D IFC represents a shift toward physics-based cytometry, where intrinsic optical properties are used to characterize cellular states in a quantitative and non-invasive manner. By complementing molecular assays with biophysical measurements, these techniques have the potential to uncover new classes of biomarkers and enable more comprehensive phenotyping of complex biological systems. Continued progress in this area will likely lead to compact, integrated systems capable of high-throughput, label-free, and volumetric analysis within lab-on-a-chip environments, aligning closely with the vision of next-generation microfluidic diagnostics.

2.3 Scattering-based 3D IFC

Scattering-based 3D IFC exploits the interaction between incident light and intrinsic refractive-index variations within cells. In conventional flow cytometry, forward- and side-scattering signals have long been used as low-dimensional indicators of cell size and internal structure, respectively.[95] Forward scattering is dominated by contributions that are relatively insensitive to internal structure, whereas scattering collected at larger angles is more sensitive to refractive-index heterogeneity and intracellular organization.[95] However, these integrated signals do not preserve spatial information and therefore cannot resolve the 3D organization of intracellular structures. Recent scattering-based IFC approaches address this limitation by combining structured illumination, spatial–temporal encoding, single-pixel detection, and computational reconstruction to recover spatially resolved scattering contrast from cells in flow (Fig. 3g–i).

An important conceptual foundation for scattering-based 3D IFC was established by spatiotemporal transformation imaging. In this framework, spatial information from a flowing cell is mapped into a time-resolved signal using a spatial filter or structured detection geometry, allowing image reconstruction with single-pixel photodetectors rather than camera-based acquisition. Han and Lo demonstrated that fluorescence and side-scattering images of rapidly flowing cells could be reconstructed from photomultiplier-tube signals, avoiding camera frame-rate limitations while maintaining cytometry-compatible throughput.[96] This strategy is particularly attractive for scattering measurements because side- and forward-scattered light can be detected with high sensitivity and temporal bandwidth using single-pixel detectors.

Building on this principle, cameraless 3D side-scattering IFC extends spatial–temporal transformation into volumetric imaging. In these systems, orthogonal light-sheet scanning or structured illumination sequentially probes different regions of the cell, while spatially encoded single-pixel detection records the corresponding side-scattering signal. Computational reconstruction then recovers 3D scattering images of individual cells in flow[25] (Fig. 3g). Therefore, in scattering-based 3D IFC, the measured time-dependent signal represents a spatially encoded projection or convolution of the underlying scattering distribution. Thus, recovery of the three-dimensional image requires inversion of this encoding process. Depending on the acquisition geometry, this recovery may involve deconvolution, back-projection, iterative optimization, or model-based inversion.[25] Regularization can be introduced to stabilize reconstruction from noisy or incompletely sampled measurements, while sparsity

constraints and learned priors may reduce the number of measurements required per cell.[38] Because side-scattering is sensitive to intracellular refractive-index heterogeneity, the reconstructed volumes provide information about subcellular organization, texture, and morphology without exogenous labels. Subsequent work combined these 3D scattering images with machine-learning analysis to classify cells from volumetric scattering fingerprints[46] (Fig. 3h). These studies demonstrated that scattering-based 3D IFC can move beyond conventional FSC/SSC intensity measurements toward high-content, label-free phenotyping.

More recently, forward-scattering implementations have further expanded the scattering-based 3D IFC toolbox. Zhou *et al.* introduced a 3D forward-scattering imaging flow cytometry system in which a needle-shaped illumination beam defines a confined interaction volume, while a micromirror-based axial scanning mechanism samples different depths within the flowing cell[38] (Fig. 3i). The detected signals are processed using spatiotemporal deconvolution to reconstruct 3D forward-scattering distributions at throughputs on the order of hundreds of cells per second. Compared with side-scattering approaches, forward-scattering emphasizes low-angle scattering components that are particularly sensitive to overall cell morphology, size, and refractive-index gradients. As a result, forward- and side-scattering 3D IFC provide complementary structural information and may be combined with other imaging channels to improve classification robustness.

Since scattering-based 3D IFC derives contrast from spatial variations in refractive index, it is closely related to the aforementioned quantitative phase and diffraction tomography approaches.[97,98] The distinction lies primarily in the measured optical information and in the objective of the reconstruction. QPI and ODT typically recover the complex optical field and use a wave-propagation model to estimate phase or, in the tomographic case, a quantitative three-dimensional RI distribution. Scattering-based approaches instead measure the redistribution of optical intensity into selected angular or spatial channels and reconstruct a volumetric scattering representation from these signals.[25,46] Consequently, scattering volumes do not generally provide a direct voxel-wise measurement of RI and are more strongly dependent on illumination and collection geometry. At the same time, this reduces the requirement for full-field interferometric detection, enabling simpler and faster acquisition architectures, including high-bandwidth single-pixel detection, which is particularly attractive for high-throughput IFC.[25]

Moreover, volumetric scattering signatures can reveal differences in cell morphology and structures associated with physiological state. Because scattering measurements can be acquired rapidly and without staining, they are attractive for high-throughput experiments and applications where fluorescence labeling is impractical or undesirable. In multimodal systems, scattering-based volumes can also be combined with transmission, fluorescence, or quantitative phase channels to link intrinsic structural information with molecular or biophysical readouts.

Despite these advantages, scattering-based 3D IFC faces important challenges in both physical interpretation and biological specificity. Scattering contrast is inherently indirect: the detected signal depends not only on the underlying cellular RI distribution but also on illumination wavelength and angle, numerical aperture, collection geometry, polarization, coherence, detector response, and the reconstruction model.[95,97,99] Different intracellular structures may therefore generate similar scattering patterns, while the same structure may produce substantially different signatures under different acquisition conditions. Multiple scattering and coherent interference further complicate the association between reconstructed scattering features and specific intracellular structures, particularly for large, optically dense, or highly heterogeneous cells. As a consequence, reconstructed scattering volumes are generally empirical structural fingerprints rather than absolute quantitative maps of specific biological components. Biological interpretation commonly relies on correlation with reference measurements, controlled perturbations, complementary imaging modalities, or data-driven classification.[46]

This dependence on acquisition geometry also poses a significant challenge for cross-platform reproducibility. Light-scattering measurements are inherently sensitive to instrument-specific parameters such as illumination wavelength, collection angle, numerical aperture, detector response, and gain, making direct comparison of uncalibrated signals across cytometers problematic.[100] Calibration against well-characterized reference particles has been shown to substantially improve cross-platform comparability of conventional flow-cytometric scattering measurements.[100] Extending analogous calibration strategies to volumetric scattering IFC, together with standardized reference samples and detailed reporting of acquisition and reconstruction parameters, will therefore be important for comparing scattering signatures and computational models across instruments.

Future progress in scattering-based 3D IFC will likely depend on tighter integration between optical design, computational reconstruction, calibration, and statistical inference. Physics-informed and inverse-scattering models could improve the interpretability of scattering measurements by more explicitly relating the detected optical signals to the underlying refractive-index distribution,[76] while machine-learning methods may enable robust classification directly from high-dimensional scattering data.[46] An equally important direction will probably be the development of calibration and harmonization strategies to improve the comparability of scattering signatures across instruments and facilitate the transfer of computational models between platforms.[100] Finally, multimodal implementations could help connect label-free structural fingerprints with biochemical identity; the combination of volumetric scattering with fluorescence has already been demonstrated

 This journal is © The Royal Society of Chemistry 2026

Table 2 Comparison of representative non-scanning 3D imaging flow cytometry implementations

Methods	Acquisition	Resolution	Throughput	Labeling	Reconstruction	Computational burden	System complexity	Applications
Multifocal etalon array (VIDA)[10]	Etalon defocus multiplexing	*XY*: 0.2–0.25 μm; *Z*: 1.5 μm	~13 objects per s	Fluorescence & brightfield	Registration then deconvolution	Low to moderate	Low – custom etalon	Nuclear morphometry & phenotyping
8-Foci multiplane imaging[101,102]	8 beams of different path length split by a prism	*XY*: 1–2 μm; *Z*: ~4.5 μm	100 volumes per s, camera limited	Fluorescence	PIV/PTV tracking; 3D localization	Moderate	High – 8-way prism & 2 synchronized cameras	Flow-field mapping; particle-flow dynamics
PSF-engineered 3D localization[16]	Astigmatic PSF encoding	*XYZ*: 160 nm	≥100 objects per s	Fluorescence	2D-Gaussian fit & depth remapping	Moderate	Low – cylindrical-lens-enabled astigmatism	Chromatin organization; NP uptake
Light-field flow cytometry (LFC)[17]	Fourier light-field; stroboscopic illumination	*XYZ*: 400–600 nm	~5750 cells per s	Fluorescence	Iterative deconvolution	High	Moderate – microlens array	Cell heterogeneity, drug delivery & response
LFC-plus[18]	Fourier light-field; stroboscopic illumination	*XY*: 4 μm, *Z*: 8 μm	~200 000 cells per s	Fluorescence	Iterative deconvolution; patch-based acceleration	High	Moderate – microlens array	Chemotherapy, cell fusion, flow migration

in imaging flow cytometry,[25] while integration with complementary modalities such as QPI, Raman spectroscopy, or downstream molecular analysis represents a promising avenue for future development. If these challenges are addressed, scattering-based 3D IFC could become a powerful complement to fluorescence- and phase-based approaches, particularly for high-throughput, label-free volumetric cytometry and morphology-guided single-cell analysis.

3 Non-scanning 3D IFC techniques

In contrast to sequential acquisition, non-scanning 3D IFC techniques enable high-speed volumetric characterization by parallelizing or computationally encoding depth information within a single or reduced exposure, encompassing multifocal, point-spread-function-engineered, and light-field modalities (Table 2).

3.1 Multifocal 3D IFC

Multifocal 3D IFC has emerged for the high-speed volumetric characterization of biological samples and fluid dynamics, overcoming the throughput limitations of traditional sequential scanning methods. By capturing multiple axial planes simultaneously in a single camera exposure, these systems enable the reconstruction of 3D information on micro- to millisecond timescales. One prominent implementation is the virtually imaged defocused array (VIDA), which utilizes a custom etalon—comprising a high-reflectivity mirror and a linear variable neutral density filter—to generate a series of reflections with distinct optical path[10] (Fig. 4a). This configuration allows for the acquisition of a complete focus stack within a single 100 μs exposure, providing an intrinsically achromatic and reconfigurable platform for high-speed 3D microscopy. As a high-throughput cytometer, the VIDA system has successfully quantified the nuclear morphology of nearly a thousand white blood cells at flow velocities of 3 mm s^{-1}, illustrating its potential for large-scale clinical and diagnostic applications.

In addition to this advancement, an 8-foci imaging platform has also been developed for precise fluidic analysis[101,102] (Fig. 4b). This approach employs a specialized prism to split incoming light into eight separate beams, each corresponding to a different focal plane, which are then recorded by synchronized sCMOS cameras. This architecture achieves exceptional spatial resolution, with single-particle tracking accuracies of approximately 10 nm laterally and 30 nm axially. Such precision has enabled the instantaneous reconstruction of 3D flow fields within complex geometries, which are essential for understanding the behavior of complex fluids in physiological environments. Together, these multifocal IFC technologies represent a significant leap forward in our ability to observe and quantify rapid volumetric processes in both life sciences and microfluidics.

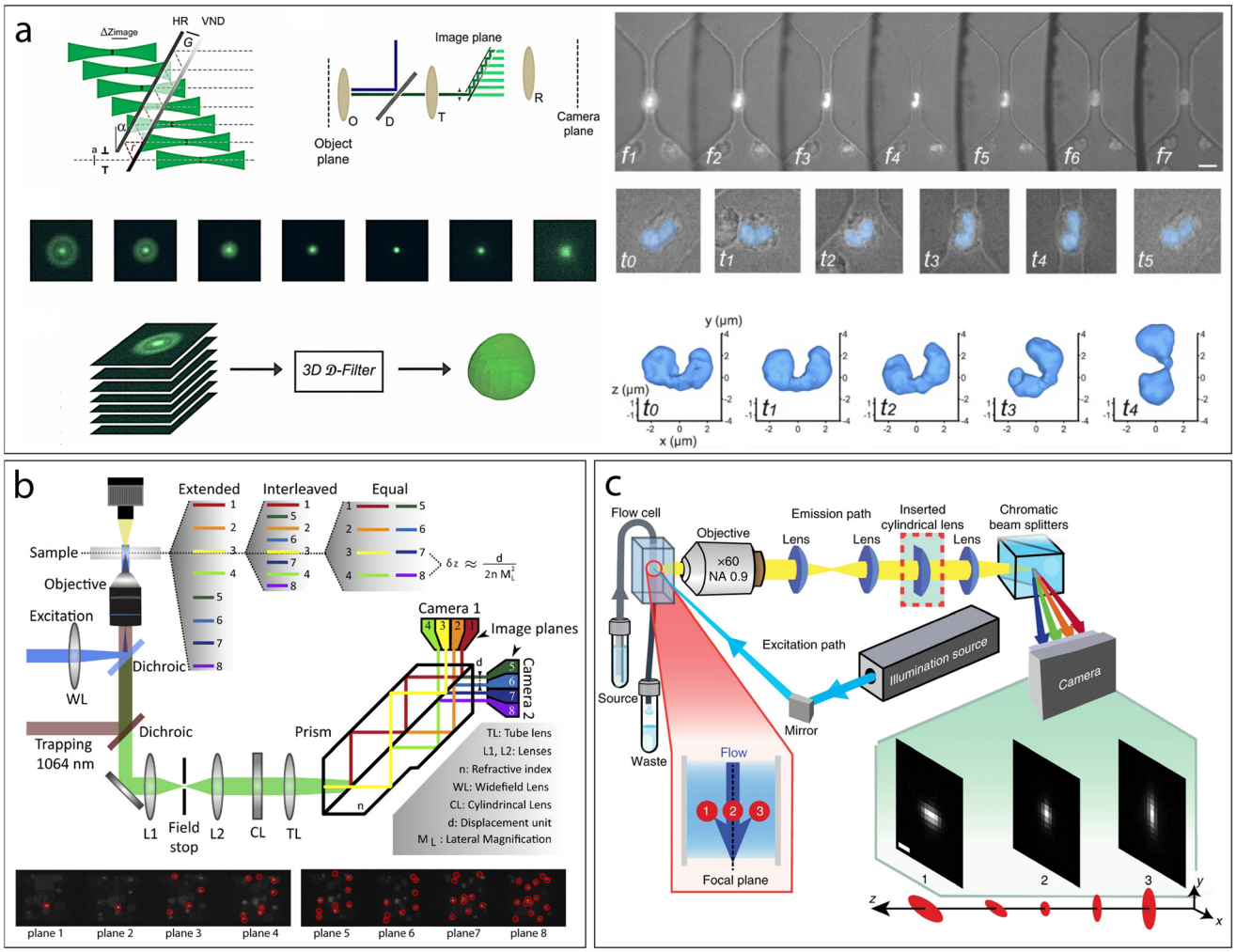


Fig. 4 Single-shot 3D imaging flow cytometry. (a) VIDA captures a multi-focal image stack of flowing cells in a single camera exposure using a custom etalon that generates multiple axially shifted reflections (reproduced from ref. 10 with permission from E. Schonbrun and G. Di Caprio, *J. Biophotonics*, Wiley-VCH, copyright 2015). (b) Simultaneous wide-field multiplane 3D imaging flow cytometry using a proprietary prism and dual-camera configuration to capture eight axially separated focal planes in a single exposure (reproduced from ref. 101 and 102 with permission from A. Gholivand *et al.*, *Phys. Fluids*, AIP Publishing, copyright 2025; and B. Louis *et al.*, *Opt. Express*, Optica Publishing Group, copyright 2020). (c) 3D localization microscopy for IFC uses engineered PSFs to encode emitter depth, enabling high-throughput, nanoscale, multicolor 3D localization of intracellular structures in flowing cells (reproduced from ref. 16 with permission from L. E. Weiss *et al.*, *Nat. Nanotechnol.*, Springer Nature, copyright 2020).

A major challenge in 3D IFC is balancing axial resolution with high throughput.[4,11,16] One strategy that addresses this issue is beam engineering, in which 3D spatial information can be encoded directly into the resulting 2D information.[103] One notable implementation of this technique combines point-spread-function (PSF) engineering with standard IFC to demonstrate high-throughput, nanoscale, multicolor 3D localization IFC[16] (Fig. 4c). The authors introduce astigmatism *via* a cylindrical lens so that each point emitter appears as an ellipse whose orientation and aspect ratio report its axial position with nanometer-scale precision after calibration. Using thousands of fluorescent beads flowing through a laminar channel, they build a depth-to-PSF-shape calibration without interrupting flow, enabling robust 3D localization across large cell populations. They achieved a throughput of 100–200 objects per s, which is orders of magnitude higher than traditional super-resolution techniques while retaining nanoscale 3D information. This work highlights the potential of PSF-engineered IFC as a powerful platform for high-throughput, nanoscale 3D cellular analysis.

3.2 Light-field flow cytometry (LFC)

Existing 3D IFC techniques remain trade-offs among spatial resolution, sequential acquisition, imaging throughput, and instrumental complexity. In recent years, however, light-field microscopy (LFM), including Fourier light-field microscopy (FLFM), or extended-depth light-field microscopy (xLFM), has emerged as a transforming volumetric imaging technique[29,104,105] capable of single-shot 3D visualization of

This journal is © The Royal Society of Chemistry 2026

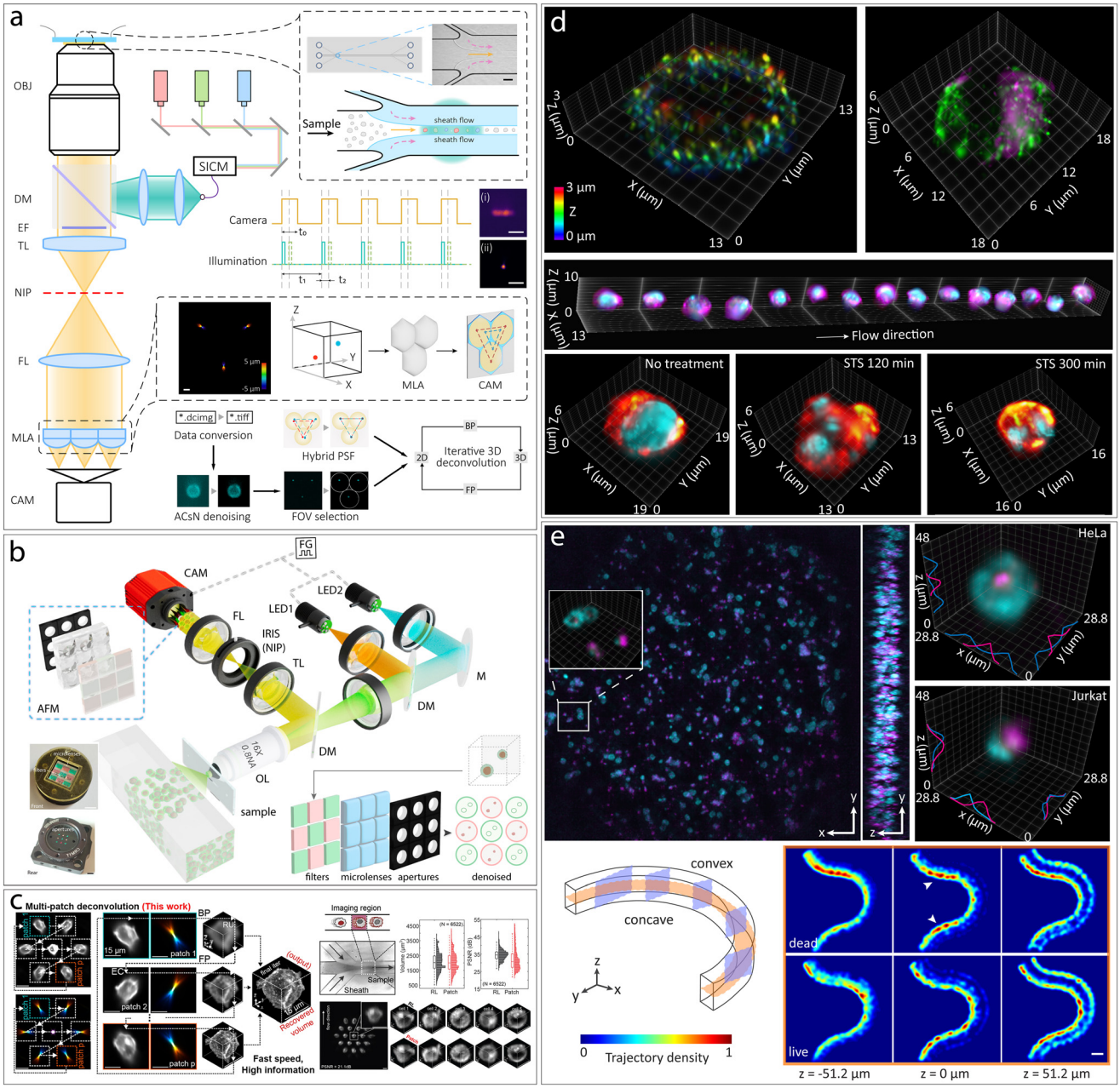


Fig. 5 Light-field flow cytometry (LFC). (a) The LFC system integrates epi-fluorescence Fourier light-field microscopy (100×), hydrodynamic flow-focusing microfluidics, and stroboscopic illumination synchronized with the laser lines and camera acquisition, enabling high-resolution, volumetric, and multiparametric 3D single-cell analysis (reproduced from ref. 17 with permission from X. Hua *et al.*, *Nat. Commun.*, Springer Nature, copyright 2024). (b) The LFC-plus system (16×) incorporates a spectral filter array for simultaneous multicolor volumetric acquisition of the flowing cells across extended, near-millimeter-scale cross-sections (reproduced from ref. 18 with permission from Z. Ling *et al.*, *Lab Chip*, Royal Society of Chemistry, copyright 2026). (c) Patch-based deconvolution accelerates volumetric reconstruction by 20–40× (reproduced from ref. 120 with permission from B. Fu *et al.*, *Biophys. J.*, Elsevier, copyright 2026). (d) The LFC platform resolved fine 3D intracellular structures, revealed cell heterogeneity, and enabled volumetric visualization of apoptosis and quantification of lipid nanoparticle-mediated mRNA delivery (reproduced from ref. 17 with permission from X. Hua *et al.*, *Nat. Commun.*, Springer Nature, copyright 2024). (e) LFC-plus enables high-throughput single-cell imaging, classification, and analysis of stiffness-dependent flow dynamics in curved microchannels (reproduced from ref. 18 with permission from Z. Ling *et al.*, *Lab Chip*, Royal Society of Chemistry, copyright 2026).

many structural-functional dynamics across various biological scales with reduced phototoxicity, high fidelity, and high scalability, facilitating investigations spanning single molecules,[106,107] living cells,[17,108–112] tissues,[113–116] and whole organisms.[117] Unlike conventional light microscopy, which records only the spatial intensity of the light field, LFM captures both spatial and angular components of the light field through a customized microlens array (MLA). This spatial-angular encoding enables computational reconstruction of volumetric information from a single 2D

camera exposure *via* wave-optics-based deconvolution.[30,114] Consequently, light-field 3D acquisition eliminates the need for axial scanning, and thereby, temporal resolution is primarily limited by camera speed rather than by mechanical sectioning or sequential imaging schemes. Such intrinsic scalability and accessibility make LFM particularly promising for next-generation 3D IFC applications.

In two recent advances, light-field flow cytometry (LFC) has been developed by integrating light-field imaging with microfluidic systems for high-throughput, high-resolution, multiparametric volumetric single-cell analysis[17,18] (Fig. 5). The initial LFC implementation demonstrated a near-diffraction-limited resolution of 400–600 nm in all three dimensions and a high throughput of up to 5750 cells per s with high-content, single-shot acquisition capabilities[17] (Fig. 5a). Subsequent refinements in LFC-plus expanded this architecture through customized spectral aperture partitioning for parallel multi-color acquisition of the 3D light field, achieving near-millimeter-scale volumetric coverage and an extended analytical imaging throughput of nearly 200 000 cells per s while maintaining a single-cell resolution in all three dimensions[18] (Fig. 5b). These modifications preserved the core light-field principle while increasing multiplexing capability, robustness, and scalability.

Grounded in an imaging-physics-driven computational pipeline, the LFC image processing integrates camera noise suppression and wave-optics-based volumetric reconstruction to enable high-resolution 3D IFC reconstruction.[109,115,118,119] Most recently, a patch deconvolution approach was developed to accelerate volumetric reconstruction by 20–40 times (achieving 100–200 events per s) without sacrificing image quality[120] (Fig. 5c). Thus, the LFC framework establishes a versatile paradigm for decoding complex biological phenomena at the single-cell level[17,18] (Fig. 5d and e).

On the other hand, there are still challenges for LFC techniques in terms of instrumentation and computation. Specifically, on the instrumentation side, trade-offs exist between resolution, field of view, imaging depth, and photon efficiency, which lead to the challenge of finding the optical configurations (*e.g.*, numerical aperture, focal length, microlens pitch size, microlens patterns, *etc.*) for optimal performance. Moreover, the fabrication and assembly of the MLA can introduce additional aberrations. Computationally, calibration procedures are applied to the processing pipeline to make up for the alignment error, aberration, and refractive-index mismatch using a hybrid PSF scheme. However, although the artifacts are greatly reduced, they are not completely removed. Meanwhile, the iterative 3D deconvolution for image reconstruction is computationally expensive and time-consuming, for which closed-loop autonomous systems have yet to be fully demonstrated, such as high-speed image-activated cell sorting. Learning-based methods are a plausible route for real-time light-field inference and can be a viable solution to enhance the capability of LFC techniques. However, they may also suffer from the inefficiency of high-quality training dataset acquisition.

Notwithstanding these remaining instrumentation and computational hurdles, rapid advancements in smart optical design, physics-informed AI reconstruction, and hardware acceleration are actively overcoming these limitations. By resolving these bottlenecks while preserving the non-invasive, single-shot 3D spatial fidelity within high-throughput flows, LFC is uniquely positioned as a robust tool for deep phenotyping and profiling, promising the application transition from fundamental single-cell discoveries to precision diagnostics and high-throughput therapeutic development.

4 Applications of 3D IFC

While the technological implementations of 3D IFC are diverse, their utility is ultimately defined by the specific biomedical and clinical questions they address. Choosing a 3D IFC modality requires balancing axial resolution, volumetric throughput, and instrumental and operational complexity against the demands of the target measurement. In this section, we summarize representative application fields of 3D IFC. These include cell and nuclear morphometry, intracellular architecture and molecular localization, label-free biophysical phenotyping, perturbation and drug-delivery assays, clinical and translational single-cell analysis, microorganisms and multicellular specimens, and microfluidic metrology. Through these representative implementations, we illustrate how 3D IFC transforms 2D cytometric investigations into volumetric quantitative metrics across diverse research pipelines (Table 3).

4.1 Single-cell morphometry and geometric phenotyping

The biological value of morphology as an independent cytometric variable has long been evident in conventional 2D IFC. Image-based morphometric features were shown to distinguish apoptotic from necrotic cells that could not be unambiguously separated using conventional fluorescence-intensity measurements alone.[35,121] Similarly, IFC enabled the analysis of molecular symmetry during mitosis, linking cell-division history with the spatial distribution of intracellular signals across statistically meaningful populations.[122]

However, 2D IFC images superimpose structures at different depths and make shape descriptors dependent on cell orientation. 3D IFC recovers the axial coordinate that remains inaccessible or ambiguous in conventional 2D IFC, and its largest biological benefit is therefore expected when cell state is encoded by 3D morphology, intracellular topology, or the relative spatial arrangement of multiple cellular structures. In fact, many descriptors of shape are intrinsically three-dimensional: parameters such as volume, surface area, sphericity, elongation, local curvature, nuclear lobulation, and the nuclear-to-cytoplasmic volume ratio cannot in general be determined unambiguously from a single 2D projection. This challenge becomes particularly

 This journal is © The Royal Society of Chemistry 2026

Table 3 Advantages, limitations, and biological applicability of the five 3D IFC macro-categories

Macro-category	Key advantages	Key limitations	Suitable applications	Limited applications
Fluorescence optical sectioning	High axial discrimination; molecular specificity; multicolor; simple reconstruction	Throughput bound by flow × camera readout; photobleaching; labeling required	Organelle morphometry; drug-induced remodeling; apoptosis; developmental models	Very large cell populations; label-free or clinically sensitive samples
Volumetric quantitative phase	Label-free without photobleaching; quantitative, physically interpretable output	Missing-cone anisotropy; single-scattering limit in thick cells; low molecular specificity	Biophysical phenotyping; nuclei and lipid droplets; disease and drug response	Specific molecular targets; optically thick, strongly scattering cells
Scattering-based	Label-free; single-pixel detection beyond camera frame rate; simple, multimodal optics	Indirect, instrument-dependent contrast; empirical fingerprints, not refractive-index maps; limited cross-platform reproducibility	Label-free classification; morphological quality control; doublets; image-activated sorting	Cross-instrument quantification; mechanistic structural interpretation
Multifocal/beam-engineering	Single-exposure volumes; no iterative reconstruction; nanoscale precision	Plane number fixed by optics; coarse axial sampling; depth calibration needed	Nuclear morphology; chromatin organization; nanoparticle uptake; particle and flow tracking	Densely labeled cytoplasm; axial detail below plane spacing
Light-field flow cytometry	Scan-free single-shot 3D imaging; near-isotropic resolution; low phototoxicity; simple instrumentation	Resolution–depth–photon trade-offs; PSF calibration; slow iterative deconvolution	Population-scale phenotyping; heterogeneity; apoptosis; mRNA delivery; chemotherapy profiling; cell flow mechanics	Finest axial detail on few cells; real-time closed-loop 3D-image-based cell sorting

relevant for cells with complex or orientation-dependent morphologies, and for experiments in which mechanical perturbations produce local deformations rather than uniform changes in projected area. 3D IFC provides a natural solution to this challenge. Early demonstrations established feasibility rather than throughput. For example, Jagannadh *et al.* introduced the slanted-channel device, which used the cell translation as a passive axial scanner to reconstruct cellular shape.[28] Quint *et al.* introduced confocal 3D IFC extended morphometry to a mechanically active readout, resolving 3D tomograms of red blood cells and their deformation under physiologically relevant flow conditions.[9]

Single-exposure architectures further made nuclear shape a practical cytometric parameter. The virtually imaged defocused array (VIDA) captures a complete focus stack, which resolved the multi-lobed 3D morphology of neutrophil nuclei as they pass through microfluidic channels and quantified the nuclear morphology of white blood cells at cytometric scale,[10] thereby enabling volumetric characterization of nuclear deformation during passage through microfluidic constrictions. Parallelized scanning reached the same goal from the opposite direction, providing volumetric phenotypes rich enough to discriminate mitotic phases in unsynchronized populations.[26,27] In particular, geometric phenotyping is not tied to fluorescent contrast. Label-free methods such as 3D forward-scattering reconstructions recover the overall morphology and size of unlabeled cells with intrinsic physical properties encoded.[38]

4.2 Biophysical phenotyping

Beyond geometry, the mechanical compliance, the dry mass and internal density, and the composition and ordering of intracellular compartments report on cell states even when staining is impractical, the environment is perturbative, or the conditions are clinically undesirable.[54,55] Unlike the observation of 3D deformed shapes alone, 3D IFC with curved and constricted microfluidic channels couples 3D shape to deformability and is able to resolve the stiffness-dependent flow behavior of individual cells,[18] linking 3D IFC to the established practice of biophysical cytometry.[55]

Besides mechanical phenotyping, optical properties of cells give access to a complementary set of quantities from how the light is transmitted and scattered. In flow-based optical diffraction tomography, the spontaneous rotation of cells in shear supplies the angular diversity required for tomographic inversion, yielding label-free 3D refractive-index maps of single cells,[37] which was later applied to studies of structures formed during blood coagulation.[66] Additionally, because refractive index is quantitative and physically interpretable, these reconstructions report dry mass, intracellular density, and internal optical heterogeneity, with sufficient intrinsic contrast to identify specific subcellular compartments without any label.[20–22] The same intrinsic signature is discriminative at the level of cell identity, where the focusing power imparted by internal compartments separates monocytes from lymphocytes without antibody staining, offering a label-free route to leukocyte subtyping.[123]

Scattering-based 3D IFC pursues the same objective through a different observable. 3D side-scattering images can be acquired without a camera while remaining compatible with simultaneous fluorescence detection,[25] and cells can be classified directly from their volumetric scattering fingerprints, which shows that label-free volumetric phenotyping does not require quantitative refractive-index recovery.[46] In contrast to refractive-index tomography,

however, reconstructed scattering volumes are not generally direct quantitative maps of a specific physical property. Rather, their values depend on experimental conditions, including reference measurements and controlled perturbations, so this method is best suited to relative comparisons, such as classification, doublet and attached-particle detection, and morphological quality control, and requires calibration against reference particles before measurements can be compared across instruments.[100]

4.3 Organelle-level intracellular architecture and nanoscale 3D localization

When biological inquiries focus on the precise spatial distribution of organelles or molecular assemblies within a cell, intracellular structural resolution becomes essential. In these contexts, the critical quantitative metric shifts from integrated signal intensity to spatial quality of the signals. Conventional planar IFC had already been applied to a broad range of such spatially resolved processes, including nuclear–cytoplasmic translocation,[124] apoptosis and cell-death morphology,[35,121] asymmetric cell division and asymmetric molecular segregation,[122] autophagy and apoptosis,[125] phagocytosis and intracellular trafficking,[126] microorganism internalization, and cell–cell interactions such as immunological synapse formation,[127] all quantified through image-based localization metrics.[128]

3D IFC expands the concepts toward quantitative analysis of the volumetric intracellular organization. Light-sheet volume cytometry achieved this in flow[12] and was advanced to reconstruction of the mitochondrial network in cancer cells[13] and to interrogation of organelles simultaneously across parallel streams with multi-sheet illumination.[15] Lattice light-sheet excitation extended such measurements to photosensitive targets that do not tolerate repeated volumetric exposure,[43] while structured illumination brought sub-diffraction intracellular detail into a chip-scale format.[7,51]

Two non-scanning strategies carry this class towards the molecular scale. PSF engineering encodes emitter depth in the shape of the PSF and has been used to quantify chromatin organization in live yeast at throughputs far above those of conventional super-resolution microscopy.[16] Light-field flow cytometry recovers near-isotropic volumes from single snapshots, resolving the 3D organization of intracellular organelles and exposing cell-to-cell heterogeneity that 2D IFC averages away.[17]

4.4 Drug delivery, cell response, and therapeutic profiling

A large fraction of 3D IFC applications concerns pharmacological perturbation experiments in which the biological readout is structurally reorganized, so that the assay requires both volumetric observation and population-scale sampling to investigate heterogeneous structural responses even within genetically similar cells. Multicolor light-sheet volume cytometry quantified drug-induced remodeling of organelle networks and apoptotic signatures across thousands of cells,[14] including changes in mitochondrial morphology following pharmacological perturbation.[15,17] Automated open-source light-sheet platforms extended the same logic to 3D cell cultures and model organisms for large-scale drug screening.[52] LFC provided volumetric visualization of apoptosis and quantified lipid-nanoparticle-mediated mRNA delivery, linking the 3D intracellular distribution of the cargo to delivery efficiency.[17] With the extended throughput, LFC-plus broadened the scope to longitudinal chemotherapeutic profiling of cancer cells and PEG-mediated cell fusion.[18] PSF-engineered 3D localization IFC mapped nanoparticle uptake and their intracellular distribution in T-lymphocyte cancer cells,[16] while holotomographic flow cytometry has been applied to drug-resistance phenotyping in a label-free context.[82] Besides pharmacological perturbations, cameraless 3D IFC has been used to quantify nuclear γH2AX foci following irradiation.[25] The number and spatial distribution of damage-associated foci represent a different biological measurement from total nuclear fluorescence and illustrate the broader importance of resolving localized responses within individual cells. Across these studies, the volumetric readout from 3D IFC strategies converts qualitative observations of drug effect or delivery efficiency into per-cell distributions, and the biological value of the measurement scales with the number of cells sampled rather than with the resolution of any individual volume.

4.5 Clinical and translational single-cell diagnostics

For clinical applications, diagnostic quantities must be derived from minimally processed samples. The acquisition and analysis must achieve sufficient throughput to resolve rare abnormal populations while ensuring high measurement interoperability, meaning that results remain consistent across different instruments and over time.[100] Therefore, volumetric single-cell measurement is especially direct. In diagnostic cytology and hematology, descriptors such as nuclear shape and lobulation, nuclear-to-cytoplasmic ratio, chromatin distribution, and blast morphology are traditionally vulnerable to projection artifacts and staining variability. Rather than introducing new biomarkers, 3D IFC transforms these established diagnostic traits into volumetric quantitative per-cell measurements.

Tomographic phase imaging combined with machine learning has been used to distinguish tumor cells from white blood cells and to discriminate among different tumor-cell types, illustrating the potential of label-free volumetric phenotyping for liquid-biopsy applications.[84] For hematologic malignancy, holo-tomographic flow cytometry has been used to characterize acute myeloid leukemia blasts and to identify quantitative three-dimensional nuclear features associated with NPM1 mutation.[19] Furthermore, evaluating these volumetric phenotypes as population distributions across thousands of cells allows for the continuous tracking of disease progression and the emergence of drug-resistant subpopulations.[83–85] For solid tumors, the clinical problem is

 This journal is © The Royal Society of Chemistry 2026

instead detection against an overwhelming normal background. Verkhovskii *et al.* recovered tumor cells from whole blood with optical-sectioning 3D IFC,[129] and Borrelli *et al.* identified ovarian cancer cells within strongly unbalanced mixed populations with holographic IFC.[130] Such measurements are informative only if enough cells are examined for the rare population to be sampled at all, which is tied to ultra-high-throughput 3D IFC implementations.[44,45] The latest advance towards clinical use has come from cytology, where cytometric imaging of whole specimens interpreted without human reading has reached clinical-grade performance in cancer screening.[131]

However, diagnosis is not the only clinical endpoint that 3D IFC techniques can support. Prognostic inference from single-cell imaging has been demonstrated in non-alcoholic steatohepatitis,[132] and label-free volumes acquired early in culture carry enough information to predict the later behavior of the same individual cells.[133] The same performance of 3D IFC can also be achieved in hematopoietic and stem-cell characterization and in cell-therapy manufacturing. Across all of these settings, what remains unproven is not imaging capability but clinical evidence, while future development should be focused on diagnostic accuracy with consecutive patient samples.

4.6 Multicellular models and whole organisms

Besides single-cell investigation, distinct works have been conducted on multicellular models or free-swimming organisms, where the volumes report the identity, organization, or behavior of the target rather than a feature inside one cell. These specimens are usually large and optically thicker than a single cell, whose phenotypes reside not only in their constituent cells but also the distribution and the arrangement of these cells. For example, light-sheet IFC platforms have provided volumetric imaging of the internal chlorophyll-a architecture of phytoplankton,[42,134] microorganisms such as *C. elegans* and zebrafish,[12,52,53] and 3D spheroids that recapitulate the *in vivo* microenvironment more faithfully than suspended single cells.[11] Ultrafast confocal IFC resolved the 3D motility of micro-organisms as they were carried through the interrogation region.[44,45] How much further this class extends is currently limited by specimen handling rather than by imaging, which requires reproducible and undamaged transportation in a controlled orientation.

4.7 Microfluidic metrology

Another practically important type of application takes the flow as the measurement target. Simultaneous multiplane imaging reconstructs instantaneous 3D flow fields from tracked tracer particles in channels that mimic vascular bifurcations, revealing transport phenomena, including radial migration and near-wall dynamics, which determine where a cell will be, and how it will be oriented.[101,102] Volumetric quantitative phase imaging has been also applied to droplets and microreactors, measuring concentration fields, mixing dynamics and interfacial behavior *in situ.*[86,87] These measurements demand absolute positional accuracy rather than molecular specificity, and they characterize the hydrodynamic environment on which every cellular measurement above implicitly depends.

5 Discussion and outlook

Driven by the fundamental need to resolve high-dimensional cellular complexity within rapid microfluidic flows, the evolution of 3D IFC has systematically confronted the trade-offs between acquisition speed, spatial resolution, and system complexity. From an engineering perspective, navigating this trade space across both scanning and non-scanning paradigms ultimately reduces to "how" depth is encoded (optical sectioning, light-field parallax, or tomographic projections), "where" the information is detected (single-pixel *vs.* camera), and "how fast" it can be decoded. These choices directly dictate the biological applicability of the system: light-sheet methods emphasize axial discrimination for fine subcellular mapping, while light-field favors single-shot simplicity at extreme velocities for massive population screening, and tomographic phase stresses phase contrast for label-free imaging. Nonetheless, practical constraints recur across modalities: (i) velocity spread and rotation (beneficial for tomography but harmful for scanning methods), (ii) spatial sampling (microlens pitch, section spacing, angular coverage), and (iii) computational bandwidth (increasing data rates driven by 3D stacks). Addressing these 3D IFC bottlenecks necessitates the next technological leap. The convergence of emerging hardware and computational innovations, including optics, engineering, and artificial-intelligence (AI) algorithms, could help overcome current spatial and computational limitations, ultimately driving the transition toward autonomous, fully integrated 3D IFC platforms.

On the hardware front, integrating ultra-thin optical metasurfaces with microfluidics offers a promising route toward compact and information-rich optical architectures for next-generation 3D IFC.[135] Metasurfaces are planar nanophotonic structures composed of subwavelength resonators that locally manipulate the phase, amplitude, polarization, and spectral response of light.[136] This capability enables multifunctional optical operations that conventionally require multiple bulky refractive or diffractive components.[137] Recent metasurface-optofluidic devices have demonstrated dynamic intensity, wavefront, and spectral control within microfluidic channels,[135] while metasurface-enabled flow cytometry systems have utilized spatial-spectral barcoding for single-shot fluorescence classification.[138] More broadly, these nanophotonic platforms allow for encoding high-dimensional optical information into camera-detectable spatial, spectral, and polarization patterns. While conventional microlens arrays have already demonstrated the value of parallelized imaging by capturing multiple microfluidic channels

across a wide field of view to maximize throughput,[139] replacing these discrete refractive arrays with planar nanophotonic elements presents an attractive direction for future 3D IFC. Beyond mere miniaturization, metasurfaces offer a unique opportunity to encode volumetric information directly within a single flat optical element. For instance, achromatic metalens arrays have demonstrated single-shot light-field imaging,[140] and light-field metasurfaces have enabled 3D particle tracking.[141] Furthermore, PSF-engineered metalenses can encode depth directly into the captured image, enabling the simultaneous recovery of intensity, depth, and polarization from a single exposure.[142] Because metasurfaces provide deterministic optical transfer functions, they can also be co-designed with computational reconstruction algorithms, as recently demonstrated by neural-network-decoded nanophotonic light-field cameras.[143] Despite these advances, implementing metasurface optics in practical 3D IFC will require addressing several open challenges, such as achieving high optical efficiency across broad fluorescence bands, maintaining stable performance over large FOVs, and robustly calibrating wavelength- and field-dependent aberrations. In this regard, the ongoing maturation of AI-enabled broadband achromatic metalens designs and scalable nanofabrication techniques, including deep-ultraviolet stepper and nanoimprint lithography, is progressively overcoming longstanding limitations in chromatic dispersion and large-area uniformity. As these design and fabrication capabilities converge, translating metasurface optics into microfluidic flow cells could provide a scalable path toward compact, manufacturable, and intrinsically three-dimensional imaging flow cytometry platforms.

Alongside these flat-optics developments, illumination and collection are moving away from fixed, mechanically actuated optics toward programmable beam shaping. Electrically tunable lenses, acousto-optic deflectors, and remote focusing, which displaces the imaged plane without moving the objective, already switch planes on microsecond to millisecond timescales in volumetric microscopy.[144] In microfluidics, they would decouple axial coverage from the mechanical constraints that currently tie the sectioning rate to the flow speed. Aberration correction is a second and largely unexplored opportunity, since refractive-index mismatch between sheath, sample, and channel wall, flow-cell manufacturing tolerances, and the refractive heterogeneity of the cells themselves all degrade the point spread function on which every volumetric reconstruction algorithm depends. Hardware adaptive optics is mature in high-resolution imaging,[145] while digital adaptive optics is more directly applicable, because it uses the angular components that a light-field or tomographic measurement already records to cancel aberrations without additional hardware.[112] A flowing cell is an unusually favorable setting for such corrections, since its static aberration can be characterized once during calibration and then applied to every subsequent event at no cost in acquisition time.

Detection is the axis on which 3D IFC is most acutely constrained. Every volumetric encoding scheme divides a fixed photon budget across planes, angular views, or microlenses, so the technique is frequently photon-starved rather than resolution-limited, and at realistic flow velocities it is sensor read noise rather than the optics that sets the practical floor. Single-photon avalanche diode (SPAD) arrays address the challenge by counting individual photons without read noise and resolve arrival times with picosecond precision,[146] and megapixel, time-gated formats are now available.[147] Photon counting relaxes the coupling between signal-to-noise ratio and flow speed, and because such an array records a decay rather than an intensity, it also makes fluorescence lifetime available as a contrast channel that is independent of fluorophore concentration and reports on the metabolic state of the cell. High-throughput lifetime flow cytometry[148,149] and light-field tomographic lifetime microscopy[150] have been demonstrated separately, and their convergence would make volumetric, lifetime-resolved IFC a realistic near-term target. Event-based sensors approach the same bottleneck from a different direction, because each pixel reports asynchronously and only when its log intensity changes, so that sparse cells against a dark background generate far less data than a frame-based camera of equivalent temporal resolution.[151] Event-based acquisition has already been used for video-activated cell sorting, where it was adopted to break the dilemma between 3D information loss and processing latency.[152] In both cases the data reduction happens at the sensor rather than downstream in software.

Parallel to these hardware innovations, the rapid development of artificial intelligence (AI) has created transformative computational capabilities to decode the massive volumetric information from the imaging data, which are increasingly integrated across 3D IFC platforms. Indeed, AI is offering new avenues for extracting rich biological information from the complex, high-dimensional data generated by 3D imaging systems. In conventional 2D IFC, AI-driven approaches have demonstrated exceptional performance for label-free cell-type identification, disease recognition, and real-time intelligent cell sorting, with convolutional neural network architectures, which have enabled accurate single-cell discrimination at the throughput of thousands of events per second.[153–156] Extending to 3D IFC, where volumetric cell images encode spatial intracellular organization, 3D morphometric fingerprints, and depth-resolved structural features that are fundamentally inaccessible from 2D projections, the AI-driven approaches substantially enrich the input information and amplify the power of single-cell analysis, providing a higher-dimensional feature space for phenotypic inference. Illustrative demonstrations include AI-driven multimodal analysis for clinical prognosis of non-alcoholic steatohepatitis from liver cell characterization,[132] and the prediction of future single-cell behaviors, such as protein expression levels and stress-induced phenotypic changes, from label-free 3D

 This journal is © The Royal Society of Chemistry 2026

images acquired at an earlier time point, achieving prediction accuracies exceeding 88%.[133] Beyond cell-type identification and classification, AI is increasingly applied to accelerate the computationally intensive volumetric reconstruction pipelines intrinsic to 3D IFC, enabling near-real-time analysis of high-content volumetric data streams.[17,157,158] The requirement becomes stricter than near-real-time whenever the instrument must act on what it sees, because a sorting decision has to be issued while the cell is still upstream of the actuator, which caps acquisition, reconstruction, inference, and actuation together at a few hundred microseconds to a few milliseconds. Two-dimensional image-activated sorting meets such budgets by moving inference onto the instrument, where field-programmable gate arrays or embedded GPUs run compressed networks.[159,160] For 3D IFC that siting is necessary but not sufficient, and an edge-resident volumetric pipeline becomes conceivable only if the reconstruction itself is reduced to a single learned forward pass in place of iterative deconvolution or Radon inversion.[161,162] Looking ahead, the development of self-supervised and weakly supervised learning frameworks that reduce dependence on exhaustive manual annotation, together with standardized benchmarking protocols and reproducible training pipelines, will be essential for translating AI-driven 3D IFC from research demonstrations toward robust clinical deployment.[158] The convergence of volumetric IFC hardware with physics-informed and data-driven AI represents a powerful and rapidly evolving axis of progress that will continue to deepen the biological and clinical insights at the single-cell level.

The advances in volumetric acquisition, system miniaturization, and AI-driven image analysis collectively chart a trajectory toward autonomous, integrated IFC platforms capable of end-to-end single-cell characterization with minimal human supervision, ranging from real-time volumetric imaging and intelligent phenotypic classification to active cell sorting and downstream biomedical intervention.[131] Extending to the 3D IFC regime, the scalability and modularity of emerging 3D IFC designs position these platforms as versatile tools across the full spectrum of biomedical inquiry. In fundamental research, 3D IFC enables investigation of dynamic cellular processes, organelle biogenesis, and population heterogeneity at previously unattainable throughput.

An important emerging direction is the extension of these capabilities beyond isolated cells toward more physiologically representative three-dimensional culture models. High-throughput volumetric analysis of adherent cells transported on hydrogel microcarriers has already enabled quantitative nuclear morphometry while preserving aspects of cell–matrix interaction,[11] illustrating a potential bridge between conventional suspension cytometry and 3D culture-based assays. However, direct applications of 3D IFC to patient-derived organoids, complex multicellular immune interactions, and host–pathogen systems remain comparatively underexplored, and represent important opportunities for future biological and translational development.

In clinical and translational settings, volumetric phenotyping is also emerging as a promising complement to conventional cytometric readouts for applications including cancer-cell identification, hematopoietic cell characterization, treatment-response assessment, and potentially stem-cell and cell-therapy quality control. In these settings, access to 3D morphology and intracellular organization may provide discriminatory information that is inaccessible from conventional 2D scatter and fluorescence measurements alone. Realizing this potential will require not only continued improvements in imaging speed, reconstruction, and automated analysis, but also validation in clinically relevant samples, standardized acquisition and analysis protocols, and integration with robust sorting and downstream workflows. The realization of compact, autonomous 3D IFC instruments that integrate volumetric imaging, real-time AI, and active cell sorting within robust, clinically deployable workflows will demand continued interdisciplinary innovation across optics, microfluidics, machine learning, and biomedical engineering. Such convergence firmly positions 3D IFC as one of the most dynamically evolving frontiers in quantitative single-cell science, with transformative potential not only for advancing our mechanistic understanding of cell biology but also for reshaping the practical landscape of precision diagnostics and targeted therapeutic development.

Author contributions

XH, BM, and ZL contributed equally to this study. SJ supervised the project. All authors contributed to the preparation of the manuscript.

Conflicts of interest

There are no conflicts to declare.

Data availability

No primary research results, software or code have been included and no new data were generated or analysed as part of this review.

Acknowledgements

We acknowledge the support of the National Science Foundation grants 2145235, 2503686, and 2607639 (to SJ), the National Institutes of Health grant R35GM124846 (to SJ), the Georgia Institute of Technology Faculty Startup Fund (to SJ), Gordon and Betty Moore Foundation GBMF ID #13829 (to HWHL), and the American Heart Association 26PRE1559643 (to ZL).

References

1 P. Rees, H. D. Summers, A. Filby, A. E. Carpenter and M. Doan, *Nat. Rev. Methods Primers*, 2022, **2**, 86.

2 M. Doan, I. Vorobjev, P. Rees, A. Filby, O. Wolkenhauer, A. E. Goldfeld, J. Lieberman, N. Barteneva, A. E. Carpenter and H. Hennig, *Trends Biotechnol.*, 2018, **36**, 649–652.
3 J. P. Robinson, G. B. Gmyrek and B. Rajwa, *BioEssays*, 2026, **48**, e70091.
4 Q. Huang, Z. Zhou, Q. Lv, Q. Min, L. Jiang, Q. Chen, J. Peng, H. Zhou, J. Zhou, Q. Dai and J. Zhou, *Front. Bioeng. Biotechnol.*, 2025, **13**, 1580749.
5 S. Dimitriadis, L. Dova, I. Kotsianidis, E. Hatzimichael, E. Kapsali and G. S. Markopoulos, *Methods Protoc.*, 2024, **7**, 28.
6 B. Mandracchia, J. Son and S. Jia, *Lab Chip*, 2021, **21**, 489–493.
7 P. Paie, G. Calisesi, A. Candeo, A. Comi, F. Sala, F. Ceccarelli, A. De Luigi, P. Veglianese, K. Muhlberger, M. Fokine, G. Valentini, R. Osellame, M. Neil, A. Bassi and F. Bragheri, *Lab Chip*, 2023, **24**, 34–46.
8 R. S. Fischer, Y. Wu, P. Kanchanawong, H. Shroff and C. M. Waterman, *Trends Cell Biol.*, 2011, **21**, 682–691.
9 S. Quint, A. F. Christ, A. Guckenberger, S. Himbert, L. Kaestner, S. Gekle and C. Wagner, *Appl. Phys. Lett.*, 2017, **111**, 103701.
10 E. Schonbrun and G. Di Caprio, *J. Biophotonics*, 2016, **9**, 1044–1049.
11 M. Yamashita, M. Tamamitsu, H. Kirisako, Y. Goda, X. Chen, K. Hattori and S. Ota, *Small Methods*, 2024, **8**, e2301318.
12 C. K. Rasmi, S. Padmanabhan, K. Shirlekar, K. Rajan, R. Manjithaya, V. Singh and P. P. Mondal, *Appl. Phys. Lett.*, 2017, 111.
13 P. Kumar, P. Joshi, J. Basumatary and P. P. Mondal, *Sci. Rep.*, 2022, **12**, 78.
14 P. Kumar and P. P. Mondal, *Sci. Rep.*, 2024, **14**, 23798.
15 P. Joshi, P. Kumar, A. S, J. M. Varghese and P. P. Mondal, *Commun. Phys.*, 2024, **7**, 25.
16 L. E. Weiss, Y. Shalev Ezra, S. Goldberg, B. Ferdman, O. Adir, A. Schroeder, O. Alalouf and Y. Shechtman, *Nat. Nanotechnol.*, 2020, **15**, 500–506.
17 X. Hua, K. Han, B. Mandracchia, A. Radmand, W. Liu, H. Kim, Z. Yuan, S. M. Ehrlich, K. Li, C. Zheng, J. Son, A. D. Silva Trenkle, G. A. Kwong, C. Zhu, J. E. Dahlman and S. Jia, *Nat. Commun.*, 2024, **15**, 1975.
18 Z. Ling, W. Liu, K. Yoon, Z. Gao, K. Han, M. Sawant, A. Kesarwala and S. Jia, *Lab Chip*, 2026, **26**, 564–575.
19 D. Pirone, C. Di Natale, M. Di Summa, N. Mosca, G. Giugliano, M. Schiavo, D. Florio, D. Marasco, P. L. Maffettone, L. Miccio, P. Memmolo and P. Ferraro, *Light: Sci. Appl.*, 2025, **14**, 233.
20 D. Pirone, J. Lim, F. Merola, L. Miccio, M. Mugnano, V. Bianco, F. Cimmino, F. Visconte, A. Montella, M. Capasso, A. Iolascon, P. Memmolo, D. Psaltis and P. Ferraro, *Nat. Photonics*, 2022, **16**, 851–859.
21 V. Bianco, M. D'Agostino, D. Pirone, G. Giugliano, N. Mosca, M. Di Summa, G. Scerra, P. Memmolo, L. Miccio and T. Russo, *et al.*, *Small Methods*, 2023, **7**, 2300447.
22 D. Pirone, D. G. Sirico, M. Mugnano, D. Del Giudice, I. Kurelac, B. Cavina, P. Memmolo, L. Miccio and P. Ferraro, *Biomed. Opt. Express*, 2022, **13**, 5585–5598.
23 M. Boutros, F. Heigwer and C. Laufer, *Cell*, 2015, **163**, 1314–1325.
24 A. Kleiber, D. Kraus, T. Henkel and W. Fritzsche, *Lab Chip*, 2021, **21**, 3655–3666.
25 Y. Han, R. Tang, Y. Gu, A. C. Zhang, W. Cai, V. Castor, S. H. Cho, W. Alaynick and Y.-H. Lo, *Optica*, 2019, **6**, 1297–1304.
26 M. Ugawa and S. Ota, *Biomed. Opt. Express*, 2022, **13**, 3647–3656.
27 M. Ugawa and S. Ota, *Small Sci.*, 2022, **2**, 2100126.
28 V. K. Jagannadh, M. D. Mackenzie, P. Pal, A. K. Kar and S. S. Gorthi, *Opt. Express*, 2016, **24**, 22144–22158.
29 M. Levoy, R. Ng, A. Adams, M. Footer and M. Horowitz, *Light field microscopy*, ACM SIGGRAPH 2006 Papers, 2006, vol. 25, pp. 924–934.
30 M. Broxton, L. Grosenick, S. Yang, N. Cohen, A. Andalman, K. Deisseroth and M. Levoy, *Opt. Express*, 2013, **21**, 25418–25439.
31 N. T. Shaked, S. A. Boppart, L. V. Wang and J. Popp, *Nat. Photonics*, 2023, **17**, 1031–1041.
32 G. Kim, H. Hugonnet, K. Kim, J.-H. Lee, S. S. Lee, J. Ha, C. Lee, H. Park, K.-J. Yoon and Y. Shin, *et al.*, *Nat. Rev. Methods Primers*, 2024, **4**, 51.
33 W. Choi, C. Fang-Yen, K. Badizadegan, S. Oh, N. Lue, R. R. Dasari and M. S. Feld, *Nat. Methods*, 2007, **4**, 717–719.
34 Y. Sung, N. Lue, B. Hamza, J. Martel, D. Irimia, R. R. Dasari, W. Choi, Z. Yaqoob and P. So, *Phys. Rev. Appl.*, 2014, **1**, 014002.
35 T. C. George, D. A. Basiji, B. E. Hall, D. H. Lynch, W. E. Ortyn, D. J. Perry, M. J. Seo, C. A. Zimmerman and P. J. Morrissey, *Cytometry, Part A*, 2004, **59**, 237–245.
36 J. Son, B. Mandracchia, A. D. Silva Trenkle, G. A. Kwong and S. Jia, *Lab Chip*, 2023, **23**, 624–630.
37 F. Merola, P. Memmolo, L. Miccio, R. Savoia, M. Mugnano, A. Fontana, G. D'Ippolito, A. Sardo, A. Iolascon, A. Gambale and P. Ferraro, *Light: Sci. Appl.*, 2017, **6**, e16241.
38 M. Zhou, J. Zhao, X. Chen, Z. Zhang, Z. Lai, Z. Zhou, A. de la Zerda and Y. H. Lo, *APL Photonics*, 2025, **10**, 126115.
39 T. Ding, K. C. M. Lee, K. K. Tsia, T. N. Siegel, D. Di Carlo and K. Goda, *Nat. Rev. Bioeng.*, 2025, **3**, 890–907.
40 D. Pirone, D. Sirico, L. Miccio, V. Bianco, M. Mugnano, P. Ferraro and P. Memmolo, *Lab Chip*, 2022, **22**, 793–804.
41 N. C. Pégard and J. W. Fleischer, *J. Biomed. Opt.*, 2013, **18**, 040503.
42 J. Wu, J. Li and R. K. Chan, *Opt. Express*, 2013, **21**, 14474–14480.
43 Y. J. Fan, H. Y. Hsieh, S. F. Tsai, C. H. Wu, C. M. Lee, Y. T. Liu, C. H. Lu, S. W. Chang and B. C. Chen, *Lab Chip*, 2021, **21**, 344–354.
44 H. Mikami, J. Harmon, H. Kobayashi, S. Hamad, Y. Wang, O. Iwata, K. Suzuki, T. Ito, Y. Aisaka, N. Kutsuna, K. Nagasawa, H. Watarai, Y. Ozeki and K. Goda, *Optica*, 2018, **5**, 117–126.
45 H. Mikami, C. Lei, N. Nitta, T. Sugimura, T. Ito, Y. Ozeki and K. Goda, *Chem*, 2018, **4**, 2278–2300.
46 R. Tang, Z. M. Zhang, X. Y. Chen, L. Waller, A. C. Zhang, J. J. Chen, Y. Y. Han, C. An, S. H. Cho and Y. H. Lo, *APL Photonics*, 2020, **5**, 126105.

 This journal is © The Royal Society of Chemistry 2026

47 M. Duocastella, G. Sancataldo, P. Saggau, P. Ramoino, P. Bianchini and A. Diaspro, *ACS Photonics*, 2017, **4**, 1797–1804.
48 Y. X. Ren, J. Wu, Q. T. K. Lai, H. M. Lai, D. M. D. Siu, W. Wu, K. K. Y. Wong and K. K. Tsia, *Light: Sci. Appl.*, 2020, **9**, 8.
49 E. J. Vargas-Ordaz, S. Gorelick, H. M. York, B. Liu, M. L. Halls, S. Arumugam, A. Neild, A. de Marco and V. J. Cadarso, *Lab Chip*, 2021, **21**, 2945–2954.
50 F. Sala, M. Castriotta, P. Paie, A. Farina, S. D'Annunzio, A. Zippo, R. Osellame, F. Bragheri and A. Bassi, *Biomed. Opt. Express*, 2020, **11**, 4397–4407.
51 F. Sala, P. Paiè, A. Candeo, F. Ceccarelli, R. Osellame, A. Bassi and F. Bragheri, *Sci. Rep.*, 2025, **15**, 11950.
52 E. J. Gualda, H. Pereira, T. Vale, M. F. Estrada, C. Brito and N. Moreno, *Biomed. Opt. Express*, 2015, **6**, 4447–4456.
53 M. Bernardello, E. J. Gualda and P. Loza-Alvarez, *Sci. Rep.*, 2022, **12**, 1969.
54 N. Lu, H. M. Tay, C. Petchakup, L. He, L. Gong, K. K. Maw, S. Y. Leong, W. W. Lok, H. B. Ong, R. Guo, K. H. H. Li and H. W. Hou, *Lab Chip*, 2023, **23**, 1226–1257.
55 T. Lee, E. H. Y. Cheung, K. C. M. Lee, D. M. D. Siu, M. C. K. Lo, E. Y. Lam, R. Goswami, S. Girardo, K. Kim, F. Reichel, M. Kubankova, M. Krater, J. Guck and K. K. Tsia, *Lab Chip*, 2025, **25**, 5329–5341.
56 J. Wiedenmann, F. Oswald and G. U. Nienhaus, *IUBMB Life*, 2009, **61**, 1029–1042.
57 P. P. Laissue, R. A. Alghamdi, P. Tomancak, E. G. Reynaud and H. Shroff, *Nat. Methods*, 2017, **14**, 657–661.
58 J. Icha, M. Weber, J. C. Waters and C. Norden, *BioEssays*, 2017, **39**, 1700003.
59 B. Ghosh and K. Agarwal, *Commun. Biol.*, 2023, **6**, 559.
60 Y. Park, C. Depeursinge and G. Popescu, *Nat. Photonics*, 2018, **12**, 578–589.
61 Z. Gorocs and A. Ozcan, *IEEE Rev. Biomed. Eng.*, 2013, **6**, 29–46.
62 P. Paie, R. Martinez Vazquez, R. Osellame, F. Bragheri and A. Bassi, *Cytometry, Part A*, 2018, **93**, 987–996.
63 J. Wu, G. Zheng and L. M. Lee, *Lab Chip*, 2012, **12**, 3566–3575.
64 W. Bishara, H. Zhu and A. Ozcan, *Opt. Express*, 2010, **18**, 27499–27510.
65 P. Memmolo, L. Miccio, F. Merola, O. Gennari, P. A. Netti and P. Ferraro, *Cytometry, Part A*, 2014, **85**, 1030–1036.
66 H. Funamizu and Y. Aizu, *J. Biomed. Opt.*, 2019, **24**, 031012.
67 J. Lim, K. Lee, K. H. Jin, S. Shin, S. Lee, Y. Park and J. C. Ye, *Opt. Express*, 2015, **23**, 16933–16948.
68 D. Pirone, P. Memmolo, F. Merola, L. Miccio, M. Mugnano, A. Capozzoli, C. Curcio, A. Liseno and P. Ferraro, *Appl. Opt.*, 2020, **60**, A277–A284.
69 E. Wolf, *Opt. Commun.*, 1969, **1**, 153–156.
70 A. J. Devaney, *Opt. Lett.*, 1981, **6**, 374–376.
71 J. Lim, A. Wahab, G. Park, K. Lee, Y. Park and J. C. Ye, *Opt. Express*, 2017, **25**, 30445–30458.
72 E. Soubies, T.-A. Pham and M. Unser, *Opt. Express*, 2017, **25**, 21786–21800.
73 S. Torino, M. Iodice, I. Rendina, G. Coppola and E. Schonbrun, *Sensors*, 2016, **16**, 1326.
74 M. M. Villone, G. D'Avino, M. A. Hulsen and P. L. Maffettone, *Phys. Rev. E: Stat., Nonlinear, Soft Matter Phys.*, 2015, **92**, 062303.
75 D. Pirone, L. Miccio, V. Bianco, P. Ferraro and P. Memmolo, *Opt. Lett.*, 2025, **50**, 6682–6685.
76 M. Lee, H. Hugonnet and Y. Park, *Optica*, 2022, **9**, 177–182.
77 S. S. Gorthi and E. Schonbrun, *Opt. Lett.*, 2012, **37**, 707–709.
78 N. C. Ruppel and M. A. Model, *Prog. Biophys. Mol. Biol.*, 2025, **198**, 1–7.
79 D. Paganin and K. A. Nugent, *Phys. Rev. Lett.*, 1998, **80**, 2586.
80 A. Sun, Y. Li, P. Zhu, X. He, Z. Jiang, Y. Kong, C. Liu and S. Wang, *Biomed. Opt. Express*, 2023, **14**, 5199–5207.
81 S. Wang, H. Huang, A. Sun, L. Zhu, W. Guo, K. Yan and L. Xue, *Sens. Diagn.*, 2024, **3**, 381–394.
82 G. Ciaparrone, D. Pirone, P. Fiore, L. Xin, W. Xiao, X. Li, F. Bardozzo, V. Bianco, L. Miccio, F. Pan, P. Memmolo, R. Tagliaferri and P. Ferraro, *Lab Chip*, 2024, **24**, 924–932.
83 D. Pirone, M. Mugnano, P. Memmolo, F. Merola, G. C. Lama, R. Castaldo, L. Miccio, V. Bianco, S. Grilli and P. Ferraro, *Nano Lett.*, 2021, **21**, 5958–5966.
84 D. Pirone, A. Montella, D. G. Sirico, M. Mugnano, M. M. Villone, V. Bianco, L. Miccio, A. M. Porcelli, I. Kurelac and M. Capasso, *et al.*, *Sci. Rep.*, 2023, **13**, 6042.
85 G. Giugliano, D. Pirone, M. Schiavo, V. Bianco, L. Miccio, P. Memmolo, G. Smaldone, G. Pecoraro, F. Altieri and M. Salvatore, *et al.*, *IEEE J. Sel. Top. Quantum Electron.*, 2025, **32**, 1–13.
86 G. Park, D. Han, G. Kim, S. Shin, K. Kim, J. K. Park and Y. Park, *Appl. Opt.*, 2017, **56**, 6341–6347.
87 Y. Hong, K. P. Dao, T. Kim, S. Lee, Y. Shin, Y. Park and D. S. Hwang, *Adv. Opt. Mater.*, 2021, **9**, 2100697.
88 D. Pirone, M. M. Villone, P. Memmolo, Z. Wang, V. Tkachenko, W. Xiao, L. Che, L. Xin, X. Li and F. Pan, *et al.*, *Opt. Lasers Eng.*, 2022, **158**, 107190.
89 Y. Jo, H. Cho, W. S. Park, G. Kim, D. Ryu, Y. S. Kim, M. Lee, S. Park, M. J. Lee and H. Joo, *et al.*, *Nat. Cell Biol.*, 2021, **23**, 1329–1337.
90 Y. Rivenson, Y. Wu and A. Ozcan, *Light: Sci. Appl.*, 2019, **8**, 85.
91 G. Kim, D. Ahn, M. Kang, J. Park, D. Ryu, Y. Jo, J. Song, J. S. Ryu, G. Choi and H. J. Chung, *et al.*, *Light: Sci. Appl.*, 2022, **11**, 190.
92 M. Lee, Y.-H. Lee, J. Song, G. Kim, Y. Jo, H. Min, C. H. Kim and Y. Park, *eLife*, 2020, **9**, e49023.
93 H. Hugonnet, M. Lee and Y. Park, *Opt. Express*, 2021, **29**, 6293–6301.
94 J. Lim, A. B. Ayoub, E. E. Antoine and D. Psaltis, *Light: Sci. Appl.*, 2019, **8**, 82.
95 M. Kerker, *Cytometry*, 1983, **4**, 1–10.
96 Y. Han and Y. H. Lo, *Sci. Rep.*, 2015, **5**, 13267.
97 K. Dong, Y. Feng, K. M. Jacobs, J. Q. Lu, R. S. Brock, L. V. Yang, F. E. Bertrand, M. A. Farwell and X.-H. Hu, *Biomed. Opt. Express*, 2011, **2**, 1717–1726.

98 Y. Sung, W. Choi, C. Fang-Yen, K. Badizadegan, R. R. Dasari and M. S. Feld, *Opt. Express*, 2009, **17**, 266–277.

99 B. Rajwa, M. Venkatapathi, K. Ragheb, P. P. Banada, E. D. Hirleman, T. Lary and J. P. Robinson, *Cytom. A: J. Int. Soc. Anal. Cytom.*, 2008, **73**, 369–379.

100 J. A. Welsh, J. C. Jones and V. A. Tang, *Cytometry, Part A*, 2020, **97**, 592–601.

101 A. Gholivand, R. Bresolí-Obach, B. Louis, K. Dahlhoff, T. Dickscheid, J. Hofkens and M. P. Lettinga, *Phys. Fluids*, 2025, **37**, 112010.

102 B. Louis, R. Camacho, R. Bresoli-Obach, S. Abakumov, J. Vandaele, T. Kudo, H. Masuhara, I. G. Scheblykin, J. Hofkens and S. Rocha, *Opt. Express*, 2020, **28**, 28656–28671.

103 B. Huang, W. Wang, M. Bates and X. Zhuang, *Science*, 2008, **319**, 810–813.

104 A. Llavador, J. Sola-Pikabea, G. Saavedra, B. Javidi and M. Martinez-Corral, *Opt. Express*, 2016, **24**, 20792–20798.

105 R. Zhao, X. Hua, W. Baek, Z. Wang, S. Jia and L. Gao, *Med X*, 2025, **3**, 25.

106 R. R. Sims, S. A. Rehman, M. O. Lenz, S. I. Benaissa, E. Bruggeman, A. Clark, E. W. Sanders, A. Ponjavic, L. Muresan, S. F. Lee and K. O'Holleran, *Optica*, 2020, **7**, 1065–1072.

107 S. Daly, J. Ferreira Fernandes, E. Bruggeman, A. Handa, R. Peters, S. Benaissa, B. Zhang, J. S. Beckwith, E. W. Sanders, R. R. Sims, D. Klenerman, S. J. Davis, K. O'Holleran and S. F. Lee, *Nat. Commun.*, 2024, **15**, 1940.

108 H. Li, C. Guo, D. Kim-Holzapfel, W. Li, Y. Altshuller, B. Schroeder, W. Liu, Y. Meng, J. B. French, K. I. Takamaru, M. A. Frohman and S. Jia, *Biomed. Opt. Express*, 2019, **10**, 29–49.

109 X. Hua, W. Liu and S. Jia, *Optica*, 2021, **8**, 614–620.

110 K. Han, X. Hua, V. Vasani, G. R. Kim, W. Liu, S. Takayama and S. Jia, *Biomed. Opt. Express*, 2022, **13**, 5574–5584.

111 Z. Ling, K. Han, W. Liu, X. Hua and S. Jia, *Biomed. Opt. Express*, 2023, **14**, 4237–4245.

112 J. Wu, Z. Lu, D. Jiang, Y. Guo, H. Qiao, Y. Zhang, T. Zhu, Y. Cai, X. Zhang, K. Zhanghao, H. Xie, T. Yan, G. Zhang, X. Li, Z. Jiang, X. Lin, L. Fang, B. Zhou, P. Xi, J. Fan, L. Yu and Q. Dai, *Cell*, 2021, **184**, 3318–3332.e3317.

113 L. Cong, Z. Wang, Y. Chai, W. Hang, C. Shang, W. Yang, L. Bai, J. Du, K. Wang and Q. Wen, *eLife*, 2017, **6**, e28158.

114 C. Guo, W. Liu, X. Hua, H. Li and S. Jia, *Opt. Express*, 2019, **27**, 25573–25594.

115 W. Liu, G. R. Kim, S. Takayama and S. Jia, *Biosens. Bioelectron.*, 2022, **208**, 114201.

116 Z. Ling, W. Liu, K. Yoon, J. Hou, P. Forghani, X. Hua, H. Yoon, M. Bagheri, L. P. Dasi, B. Mandracchia, C. Xu, S. Nie and S. Jia, *Nat. Cardiovasc. Res.*, 2025, **4**, 637–648.

117 K. C. Zhou, C. Cook, A. Chakraborty, J. Bagwell, J. Jonsson, K. C. Lee, X. Yang, S. Xu, R. Balla, K. Kolar, C. Lewis, M. Harfouche, D. T. Fox, M. Bagnat and R. Horstmeyer, *Optica*, 2025, **12**, 674–684.

118 B. Mandracchia, X. Hua, C. Guo, J. Son, T. Urner and S. Jia, *Nat. Commun.*, 2020, **11**, 94.

119 B. Mandracchia, W. Liu, X. Hua, P. Forghani, S. Lee, J. Hou, S. Nie, C. Xu and S. Jia, *Sci. Adv.*, 2023, **9**, eadg9245.

120 B. Fu, C. L. Jones, D. Heraghty, S. Yang, C. O'Brien-Ball, V. Junghans, H. Yang, D. Klenerman, T. P. J. Knowles, L. E. Weiss, R. A. Fernandes and S. F. Lee, *Biophys. J.*, 2026, **5**, 1305–1314.

121 S. Henery, T. George, B. Hall, D. Basiji, W. Ortyn and P. Morrissey, *Apoptosis*, 2008, **13**, 1054–1063.

122 A. Filby, E. Perucha, H. Summers, P. Rees, P. Chana, S. Heck, G. M. Lord and D. Davies, *Cytometry, Part A*, 2011, **79**, 496–506.

123 J. Behal, D. Pirone, D. Sirico, V. Bianco, M. Mugnano, D. Del Giudice, B. Cavina, I. Kurelac, P. Memmolo, L. Miccio and P. Ferraro, *Cytometry, Part A*, 2023, **103**, 251–259.

124 T. C. George, S. L. Fanning, P. Fitzgerald-Bocarsly, R. B. Medeiros, S. Highfill, Y. Shimizu, B. E. Hall, K. Frost, D. Basiji, W. E. Ortyn, P. J. Morrissey and D. H. Lynch, *J. Immunol. Methods*, 2006, **311**, 117–129.

125 C. de la Calle, P. E. Joubert, H. K. Law, M. Hasan and M. L. Albert, *Autophagy*, 2011, **7**, 1045–1051.

126 A. Ploppa, T. C. George, K. E. Unertl, B. Nohe and M. E. Durieux, *Scand. J. Clin. Lab. Invest.*, 2011, **71**, 362–369.

127 F. Ahmed, S. Friend, T. C. George, N. Barteneva and J. Lieberman, *J. Immunol. Methods*, 2009, **347**, 79–86.

128 N. S. Barteneva, E. Fasler-Kan and I. A. Vorobjev, *J. Histochem. Cytochem.*, 2012, **60**, 723–733.

129 R. A. Verkhovskii, A. A. Kozlova, O. A. Sindeeva, I. O. Kozhevnikov, E. S. Prikhozhdenko, O. A. Mayorova, O. V. Grishin, M. A. Makarkin, A. V. Ermakov, A. S. Abdurashitov, V. V. Tuchin and D. N. Bratashov, *Biomed. Opt. Express*, 2021, **12**, 380–394.

130 F. Borrelli, J. Behal, A. Cohen, L. Miccio, P. Memmolo, I. Kurelac, A. Capozzoli, C. Curcio, A. Liseno, V. Bianco, N. T. Shaked and P. Ferraro, *APL Bioeng.*, 2023, **7**, 026110.

131 N. Nitta, Y. Sugiyama, T. Sugimura, T. Ito, K. Ikebata, H. Abe, S. Ishii, H. Kanao, N. Hosoya, R. U. Islam, A. Jain, M. Hasani, J. Zonghi, P. Koh, Y. Mase, M. Kanematsu, N. M. Z. Ali, Y. Murata, A. Shikama, Y. Kobayashi, D. Matsubara, Y. Himeji, H. Nakamura, A. Hashizume, M. Umemori, H. Ohsaki, Y. Luo, T. Ding, F. C. Schmitt, R. Y. Osamura, T. Chiba and K. Goda, *Nature*, 2026, **651**, 472–481.

132 R. Subramanian, R. Tang, Z. Zhang, V. Joshi, J. N. Miner and Y. H. Lo, *Sci. Rep.*, 2022, **12**, 11180.

133 Z. Zhang, Y. Zhu, Z. Lai, M. Zhou, X. Chen, R. Tang, W. Alaynick, S. H. Cho and Y. H. Lo, *Sci. Rep.*, 2025, **15**, 5715.

134 E. J. Gualda, H. Pereira, G. G. Martins, R. Gardner and N. Moreno, *Cytometry, Part A*, 2017, **91**, 144–151.

135 Q. Li, J. van de Groep, A. K. White, J. H. Song, S. A. Longwell, P. M. Fordyce, S. R. Quake, P. G. Kik and M. L. Brongersma, *Nat. Nanotechnol.*, 2022, **17**, 1097–1103.

136 N. Yu and F. Capasso, *Nat. Mater.*, 2014, **13**, 139–150.

137 X. Zou, R. Lin, Y. Fu, G. Gong, X. Zhou, S. Wang, S. Zhu and Z. Wang, *Adv. Opt. Mater.*, 2023, **12**, 2203149.

138 T. Hong, D. Li and J. G. Valentine, *Optica*, 2024, **11**, 577–582.

 This journal is © The Royal Society of Chemistry 2026

139 G. Holzner, Y. Du, X. Cao, J. Choo, A. J. deMello and S. Stavrakis, *Lab Chip*, 2018, **18**, 3631–3637.

140 R. J. Lin, V. C. Su, S. Wang, M. K. Chen, T. L. Chung, Y. H. Chen, H. Y. Kuo, J. W. Chen, J. Chen, Y. T. Huang, J. H. Wang, C. H. Chu, P. C. Wu, T. Li, Z. Wang, S. Zhu and D. P. Tsai, *Nat. Nanotechnol.*, 2019, **14**, 227–231.

141 A. L. Holsteen, D. Lin, I. Kauvar, G. Wetzstein and M. L. Brongersma, *Nano Lett.*, 2019, **19**, 2267–2271.

142 Z. Shen, F. Zhao, C. Jin, S. Wang, L. Cao and Y. Yang, *Nat. Commun.*, 2023, **14**, 1035.

143 Q. Fan, W. Xu, X. Hu, W. Zhu, T. Yue, C. Zhang, F. Yan, L. Chen, H. J. Lezec, Y. Lu, A. Agrawal and T. Xu, *Nat. Commun.*, 2022, **13**, 2130.

144 U. L. Bohm and B. Judkewitz, *Nat. Commun.*, 2024, **15**, 9555.

145 K. M. Hampson, R. Turcotte, D. T. Miller, K. Kurokawa, J. R. Males, N. Ji and M. J. Booth, *Nat. Rev. Methods Primers*, 2021, **1**, 68.

146 C. Bruschini, H. Homulle, I. M. Antolovic, S. Burri and E. Charbon, *Light: Sci. Appl.*, 2019, **8**, 87.

147 K. Morimoto, A. Ardelean, M.-L. Wu, A. C. Ulku, I. M. Antolovic, C. Bruschini and E. Charbon, *Optica*, 2020, **7**, 346–354.

148 H. Kanno, K. Hiramatsu, H. Mikami, A. Nakayashiki, S. Yamashita, A. Nagai, K. Okabe, F. Li, F. Yin, K. Tominaga, O. F. Bicer, R. Noma, B. Kiani, O. Efa, M. Buscher, T. Wazawa, M. Sonoshita, H. Shintaku, T. Nagai, S. Braun, J. P. Houston, S. Rashad, K. Niizuma and K. Goda, *Nat. Commun.*, 2024, **15**, 7376.

149 J. Rottmann, N. Schierbaum, A. Netaev, M. Ligges and K. Seidl, *Curr. Dir. Biomed. Eng.*, 2023, **9**, 363–366.

150 Y. Ma, J. Park, L. Huang, C. Sen, S. Burri, C. Bruschini, X. Yang, Q. Cui, R. B. Cameron, G. A. Fishbein, B. N. Gomperts, A. Ozcan, E. Charbon and L. Gao, *Proc. Natl. Acad. Sci. U. S. A.*, 2024, **121**, e2402556121.

151 G. Gallego, T. Delbruck, G. Orchard, C. Bartolozzi, B. Taba, A. Censi, S. Leutenegger, A. J. Davison, J. Conradt, K. Daniilidis and D. Scaramuzza, *IEEE Trans. Pattern Anal. Mach. Intell.*, 2022, **44**, 154–180.

152 W. He, J. Zhu, Y. Feng, F. Liang, K. You, H. Chai, Z. Sui, H. Hao, G. Li, J. Zhao, L. Deng, R. Zhao and W. Wang, *Nat. Commun.*, 2024, **15**, 10792.

153 N. Nitta, T. Sugimura, A. Isozaki, H. Mikami, K. Hiraki, S. Sakuma, T. Iino, F. Arai, T. Endo, Y. Fujiwaki, H. Fukuzawa, M. Hase, T. Hayakawa, K. Hiramatsu, Y. Hoshino, M. Inaba, T. Ito, H. Karakawa, Y. Kasai, K. Koizumi, S. Lee, C. Lei, M. Li, T. Maeno, S. Matsusaka, D. Murakami, A. Nakagawa, Y. Oguchi, M. Oikawa, T. Ota, K. Shiba, H. Shintaku, Y. Shirasaki, K. Suga, Y. Suzuki, N. Suzuki, Y. Tanaka, H. Tezuka, C. Toyokawa, Y. Yalikun, M. Yamada, M. Yamagishi, T. Yamano, A. Yasumoto, Y. Yatomi, M. Yazawa, D. Di Carlo, Y. Hosokawa, S. Uemura, Y. Ozeki and K. Goda, *Cell*, 2018, **175**, 266–276.e213.

154 Y. Li, A. Mahjoubfar, C. L. Chen, K. R. Niazi, L. Pei and B. Jalali, *Sci. Rep.*, 2019, **9**, 11088.

155 Y. Gu, A. Chen, X. Zhang, C. Fan, K. Li and J. Shen, *ASP Trans. Pattern Recognit. Intell. Syst.*, 2021, **1**, 18–27.

156 S. B. Luo, Y. Z. Shi, L. K. Chin, P. E. Hutchinson, Y. Zhang, G. Chierchia, H. Talbot, X. D. Jiang, T. Bourouina and A. Q. Liu, *Adv. Intell. Syst.*, 2021, **3**, 2100073.

157 D. M. D. Siu, K. C. M. Lee, B. M. F. Chung, J. S. J. Wong, G. Zheng and K. K. Tsia, *Lab Chip*, 2023, **23**, 1011–1033.

158 P. Pozzi, A. Candeo, P. Paie, F. Bragheri and A. Bassi, *Front. Bioinform.*, 2023, **3**, 1229052.

159 R. Tang, L. Xia, B. Gutierrez, I. Gagne, A. Munoz, K. Eribez, N. Jagnandan, X. Chen, Z. Zhang, L. Waller, W. Alaynick, S. H. Cho, C. An and Y. H. Lo, *Biosens. Bioelectron.*, 2023, **220**, 114865.

160 H. Li, J. Bai, X. Ma, L. Li, Y. Liu, X. Liu, S. Shen and C. Lim, *Sci. Adv.*, 2025, **11**, eaea6007.

161 F. Borrelli, J. Behal, V. Bianco, A. Capozzoli, C. Curcio, A. Liseno, L. Miccio, P. Memmolo and P. Ferraro, *Opt. Lasers Eng.*, 2024, **172**, 107873.

162 Z. Lu, M. Jin, S. Chen, X. Wang, F. Sun, Q. Zhang, Z. Zhao, J. Wu, J. Yang and Q. Dai, *Nat. Methods*, 2025, **22**, 1545–1555.